Subduction zone guided waves and the heterogeneity structure of the subducted plate: Intensity anomalies in northern Japan

T. Furumura
Earthquake Research Institute, University of Tokyo, Tokyo, Japan

B. L. N. Kennett
Research School of Earth Sciences, Australian National University, Canberra ACT, Australia

Received 7 October 2004; revised 12 April 2005; accepted 1 June 2005; published 12 October 2005.

[1] The subducting Pacific plate acts an efficient waveguide for high-frequency signals and often produces anomalously large intensity on the eastern seaboard of northern Japan during deep earthquakes. The waveform records in the region of high intensity show a low-frequency ($f < 0.25$ Hz) onset for both P and S waves, followed by large, high-frequency ($f > 2$ Hz) later arrivals with a long coda. This behavior is not explained by a simple subduction zone model comprising a high-velocity plate with low attenuation. From the analysis of observed broadband waveforms and numerical simulation of seismic wave propagation in the Pacific subduction zone we demonstrate that the high-frequency guided waves traveling in the subducting plate arise from the scattering of seismic waves by heterogeneity in plate structure. Our preferred model of the heterogeneity has elongated scatterers parallel to the plate margin described by a von Karmann function with a downdip correlation length of about 10 km and much shorter correlation length of about 0.5 km in thickness. The standard deviation of wave speed fluctuations from the averaged background model is about 2%. This new heterogeneous plate model generates significant scattering of seismic waves with wavelengths shorter than correlation distance in thickness, but low-frequency waves, with long wavelengths, can easy tunnel through such lamina structure. The result is frequency-selective propagation characteristics with a faster low-frequency phase followed by large and high-frequency signals with very long coda. A low-wave speed channel effect from the former oceanic crust at the top of the subducting slab is not necessary to explain the observed dispersed signals and the very long high-frequency coda. Three-dimensional simulations, using the Earth simulator supercomputer for modeling of high-frequency seismic wave propagation in the Pacific subduction zone including plate heterogeneity, clearly demonstrate the scattering waveguide effects for high-frequency seismic waves traveling in the plate. The region of large intensity for the heterogeneous model migrates away from the hypocenter into northern Japan with an elongated zone along the Pacific coast, almost comparable to the observations from deep events in the Pacific plate.

Citation: Furumura, T., and B. L. N. Kennett (2005), Subduction zone guided waves and the heterogeneity structure of the subducted plate: Intensity anomalies in northern Japan, *J. Geophys. Res.*, *110*, B10302, doi:10.1029/2004JB003486.

1. Introduction

[2] Anomalously large shocks are often observed on the eastern seaboard (Pacific coast) of northern Japan from deep earthquakes occurring within the Pacific plate. Sometimes the events are not felt near the epicenter, but many people are surprised by large and long ground shaking from such deep and distant earthquakes.

[3] The abnormal intensities in northern Japan from events beneath the Japan Sea has been recognized since the first extensive set of seismic observations was started in Japan by the Japan Meteorological Agency (JMA) in the early 1900s [e.g., *Hasegawa*, 1918; *Ishikawa*, 1926a, 1926b; *Wadati*, 1928; *Ishikawa*, 1930]. *Ishikawa* [1933] noticed that the large intensity region is clearly related to the area of early seismic wave arrivals but with no clear relation to surface geology. He indicated that there needed to be large-scale anomalies in crust and mantle structure rather than in the shallow structure which can produce localized site amplification effects as, e.g., in sedimentary basins.

[4] Although the observations were quite clear, no satisfactory explanation for the cause of anomalous intensity was made for over 30 years. *Utsu* [1966] was the first to

0148-0227/05/2004JB003486$09.00

explain the cause of the anomalous intensity pattern using a model of the absorption structure of the earthquake zone in northern Japan with a low attenuation (high Q) dipping seismic layer and a high attenuation (low Q) upper mantle above the seismic layer. He also noted that the dipping high-Q seismic layer shows higher wave speed than the adjacent low-Q and low-wave speed upper mantle [*Utsu*, 1967]. *Utsu and Okada* [1968] analyzed a number of waveform records and suggested that the Q values for the seismic layer needed to be at least ten times larger than those for the surrounding mantle in order to explain the distorted intensity pattern. The high-Q and high-wave speed seismic layer descending beneath northern Japan discussed by *Utsu* [1966] is now recognized as the expression of the subducted Pacific plate.

[5] Another notable feature of the records from such deep events in the Pacific plate, which produce large intensities along the eastern seaboard of northern Japan, is that the seismograms show a low-frequency (f < 0.25Hz) onset followed by a large-amplitude high-frequency (f > 2Hz) signal [e.g., *Iidaka and Mizoue*, 1991; *Abers*, 2000]. The arrival time of the low-frequency precursor corresponds to the standard travel time table for deep subduction events in northern Japan, but the high-frequency second arrival is delayed by about 1 to 2 s. The observation of separation of the low- and high-frequency components in the waveforms from deep events is a common characteristic where there has been a significant distance of propagation in the subducting plate. Examples have been reported for major subduction zones such as the Nazca plate in South America [*Snoke et al.*, 1974; *Martin et al.*, 2003], the Vanuatu region [*Chiu et al.*, 1985], and the Cocos plate off Nicaragua [*Abers et al.*, 2003], and the Mariana basin [*Ouchi*, 1981] that indicate common characteristics in the heterogeneous structure of the subducted oceanic plate.

[6] By understanding the observed waveforms and the way in which large intensity signals with high frequency are guided from source to receiver we can gain information on the detailed structure of the subducting plate, and subduction process.

[7] Several studies have considered the trapping of waves in the waveguide formed by the thin, low-wave speed zone corresponding to the former oceanic crust at the top of the plate as an explanation of the separation of the low-frequency arrivals and the high-frequency waves with a long coda [*Abers*, 2000; *Abers et al.*, 2003; *Martin et al.*, 2003]. This former oceanic crust layer in the plate often acts as an efficient waveguide for high-frequency waves when the earthquakes occur inside the low-wave speed layer; typical examples were observed in the Philippine sea plate subducting beneath western Japan for earthquakes no deeper than 60 km [*Fukao et al.*, 1983; *Hori et al.*, 1985; *Oda et al.*, 1990]. Recent studies employing receiver function techniques have also succeeded in imaging the low-wave speed oceanic crustal layer at the Nazca plate down to 120 km depth [*Yuan et al.*, 2000] and in the Pacific plate beneath central Alaska near 150 km depth [*Ferris et al.*, 2003]. However, the direct application of such a guided wave effect to the observations for deep (h > 200–500 km) Pacific plate earthquakes would be difficult because the low-wave speed former oceanic layer may not be able to survive beyond a depth of about 110 km without change, because the dehydrated material at that depth is expected to transform to a high wave speed ecologite. On the basis of an S-to-P wave-converted phase at the top of the subducting Pacific plate in northern Japan, *Matsuzawa et al.* [1987] also support the concept that the low-wave speed former oceanic layer does not extend to depths deeper than 110–160 km. Other explanations given for the origin of the high-frequency later phases are a reflection at the top of the plate [*Snoke et al.*, 1974] or a reflection from an interface inside the plate [*Iidaka and Mizoue*, 1991], but these models cannot explain the long duration and delay of the high-frequency signals.

[8] We present an alternative explanation of the waveguide effects in the subducting plate that can explain the features of the deep plate events with their low-frequency onset and the following burst of higher-frequency P and S waves with an extensive coda. In this new model, the character of the broadband waveforms in northern Japan, particularly the guiding of high-frequency energy, is produced by internal scattering from fluctuations in the elastic parameters inside the plate. We show that a preferred model for the properties of the subducting Pacific plate is stochastic heterogeneity of P and S wave velocity and density described by a von Karmann distribution with a longer correlation length (~10 km) in the downdip direction along the subducting plate and a shorter correlation length (~0.5 km) in thickness. The standard deviation of the fluctuations is about 2% of the averaged background properties.

[9] Numerical two-dimensional (2-D) simulation of seismic wave propagation using parallel computation with a higher-order finite difference method allows modeling of high-frequency seismic waves up to 18 Hz. The simulations demonstrate that such elongated scatterers inside the dipping plate can act as an efficient waveguide for higher-frequency seismic waves with a long coda generated by multiple scattering. Low-frequency waves are relatively insensitive to the presence of such heterogeneity, due to the effects of wave front healing and leakage through the lamella structures [*Fuchs*, 1977]. Numerical simulation demonstrates that splitting of high- and low-frequency waves occurs only for elongated scatterers, but not for isotropic scatterers. The curvature of the subducted plate as it approaches the trench allows the guided energy to escape and be recorded at stations along the coastline to the east of the volcanic front.

[10] Further insight into the generation of the patterns of anomalous intensity associated with deep events in northern Japan can be found with 3-D numerical simulation using large-scale parallel finite difference computation on the Earth simulator supercomputer. We are able to build a realistic 3-D model of the crust, mantle and subduction zone structure for central Japan including plate heterogeneity and use this to follow the complex pattern of seismic wave propagation from a deep subduction zone event. Calculations can be carried to an upper frequency of 3 Hz and so provide a good representation of the major features of the observed broadband waveforms and the distorted patterns of seismic intensity.

2. Abnormal Intensity From Deep Seismic Events in the Subducted Plate

[11] Figure 1 illustrates examples of seismic intensity patterns using the seven point scale of the Japan Meteoro-

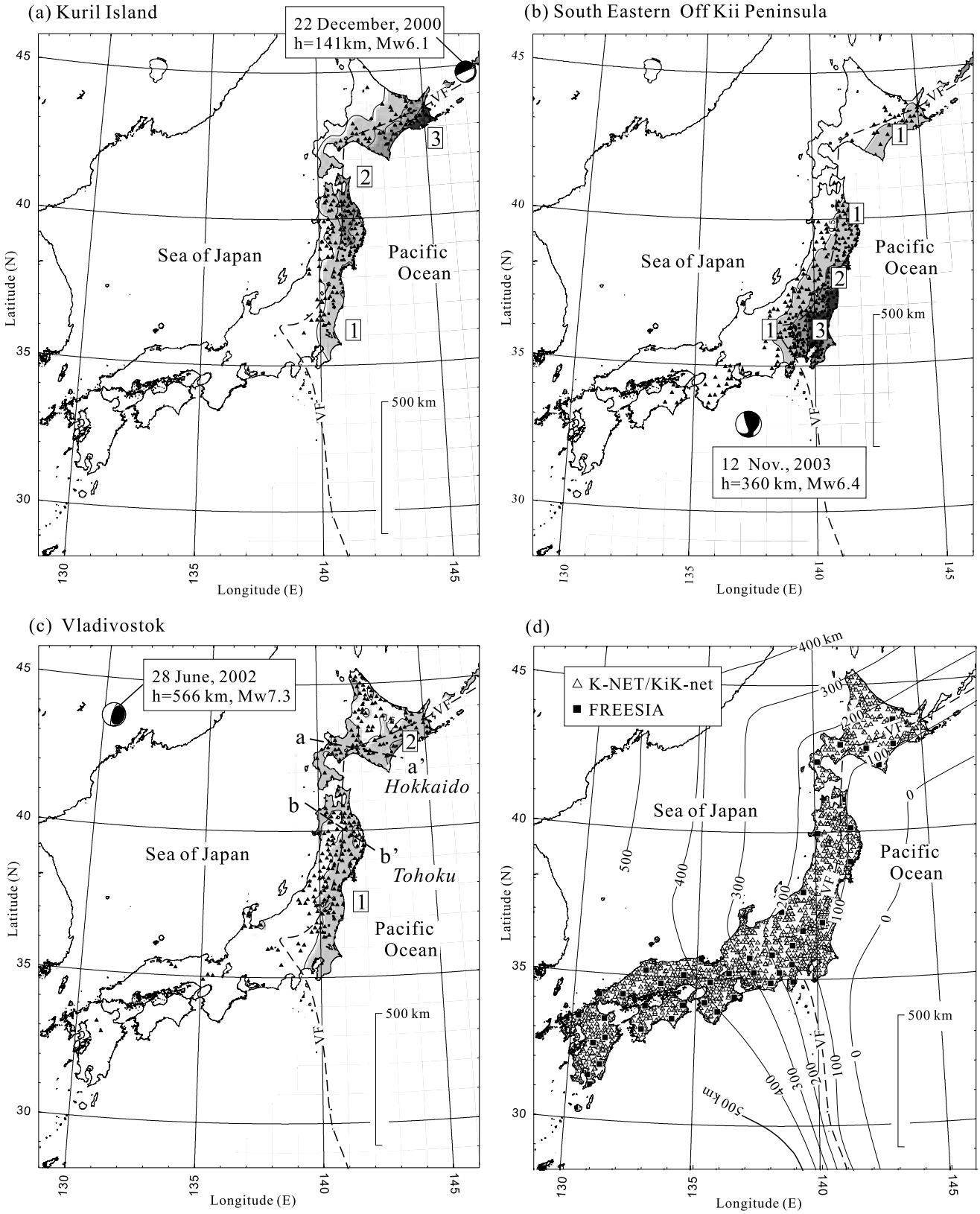

Figure 1. Example of anomalous intensity pattern for deep focus earthquakes (a) Kuriles, (b) off southeast Kii Peninsula, (c) Vladivostok, and (d) the coverage of strong motion instruments (K-NET and KiK-net, triangles) and the FREESIA broadband stations (squares) together with the configuration of the Pacific plate. The dashed line indicates the volcanic front (VF). The solid triangles in Figures 1a–1c indicate the triggering pattern of the strong motion instruments produced by the earthquakes.

logical Agency (JMA) for earthquakes occurring in the subducting Pacific plate. The patterns for each of the events show a substantial north-south elongation with a concentration of intensity along the eastern seaboard of Japan which lies several hundred kilometers from the hypocenters. These intensity maps are produced from the three-component accelerograms of the nationwide K-NET and KiK-net stations (Figure 1d). The JMA intensity is calculated for each station and the intensity pattern is then interpolated using a cubic spline function. The triggering pattern of the K-NET and the KiK-net strong motion instruments illustrated in Figures 1a–1c roughly outlines the felt area (JMA intensity 1) during the earthquakes.

[12] The JMA seismic intensity scale was originally defined from felt reports of the strength of ground shaking and the damage rate of wooden frame houses. The modern intensity measurement system follows the same scale using three-component ground accelerations and appropriate band-pass filters; so that anomalies in ground motion are more significant in high-frequency ground acceleration for frequencies above 1 Hz. The anomalous pattern is therefore prominent when we map the peak ground acceleration of the event. However, the level of the anomaly is quite mild for peak ground displacement.

[13] The larger seismic intensity from the three illustrated events is concentrated to the east of the volcanic front in northern Japan associated with the subducting Pacific plate. A remarkable extension of intensity on the Pacific Ocean side of northern Japan is seen in the intensity map for the event in the Kuriles Figure 1a. The felt area extends from the hypocenter to central Japan, several hundred kilometers from the hypocenter of the M_w 6.1 event. The radiation of high-frequency S wave signals over 2 Hz is considered to be almost isotropic, and so it is not a major cause of the distorted intensity patterns. Even though the intensity is strongly influenced by the site amplification effect at each of the stations but the large extent of the anomalous intensity pattern is not explained by the geological conditions at each of the seismometer locations.

[14] A similar anomalous pattern to the Kuriles event is found for an event beneath southeast of Kii Peninsula (h = 360 km; M_w 6.4) which occurred deep in the Pacific plate (Figure 1b). Even considering the relatively large magnitude it is surprising to find that the area of felt ground shaking from such a deep and distant earthquake covers almost the whole extent of the Pacific coast of northern Japan, but no anomalous intensities are found in the area above the source.

[15] Figure 1c depicts another example of an anomalous intensity pattern from a deep event near Vladivostok (h = 566 km; M_w 7.3). No significant intensity was reported above the epicenter during the deep earthquake, but large ground motion with maximum intensity 2 was observed at the Pacific Ocean side of northern Japan in a zone which runs for several hundred kilometers from north to south.

[16] These anomalous patterns of seismic intensity are characteristic of all deep earthquakes in the subducting Pacific plate, but do not occur for shallow crustal earthquakes in northern Japan. Thus the large-scale patterns of anomalous intensity shown in Figures 1a–1c indicate the presence of strong contrasts in the efficiency of wave propagation through the upper mantle and the subduction zone, rather than localized site amplification effects such as those due to sedimentary basins.

[17] Figure 2 displays three-component accelerograms of the KiK-net borehole stations from the Vladivostok event (Figure 1c) along profiles from the Japan Sea side to the Pacific Ocean side (back arc to forearc) in Hokkaido (a–a′) and Tohoku (b–b′). The traces are multiplied by the epicentral distance to provide a rough compensation for geometrical spreading. With the borehole sensors the localized amplification effects in shallow sedimentary layers and topography effect are minimized, and so we can make a direct comparison of the amplitude of the waveforms at the different stations. The contrast in amplitude across the volcanic front is striking, with rather complex records observed close to the Pacific coast. There is significant P wave energy on the transverse components to the paths indicating complex wave propagation from the source to the receivers.

[18] The two profiles of three-component accelerograms in Hokkaido and Tohoku show considerable variation in the character of the seismic wave field between the forearc (east) and the back arc sides of the volcanic front. This is due to efficient propagation of seismic waves to the forearc side along the subducting high-Q and high- wave speed Pacific plate and dramatic attenuation of seismic waves on the back arc side when they pass through the low-Q and low-wave speed mantle wedge above the subduction zone. The high frequency P and S waves with dominant frequency of a few Hz in the waveforms of the forearc stations have a rapid early increase in amplitude followed by a slow decline into the coda; it is difficult to identify the onset of the S phase because it is overridden by the large P wave coda. However, there is a strong with the weak and low-frequency waveforms at the back arc stations, where the S waves are not very distinct.

[19] We compare the differences in the frequency contents at forearc and back arc stations in northern Japan, using the broadband waveforms at the FREESIA stations HSS and KMU, which are both rock sites (the station locations are shown in Figure 3). Figure 4 shows the three-component broadband waveform from the 2 February 2002 Vladivostok event (event C, M_w 5.9, h = 400 km), recorded at both a forearc station (KMU) and a back arc station (HSS). There is a pronounced contrast in the visual appearance of the seismograms in frequency content and duration, with much higher frequencies at KMU. The Fourier spectrum of the P and S waves at KMU and HSS are compared in Figure 5 for a short time window of 6.4 s on the vertical component for P, and 12.8 s on the transverse component for S waves. The spectra are scaled by the epicentral distance to partially compensate for geometrical spreading.

[20] The elevated high-frequency spectrum of KMU relative to HSS for the P wave covers the range from 1 to over 20 Hz with a generally smooth behavior. The spectral ratio of the ground motions at KMU relative to HSS increases rapidly with increasing frequency with an increase from a factor of 10 at 4 Hz to over 100 at 20 Hz. The sudden decay in the relative amplification at KMU for frequencies above 20 Hz is due to increasing noise in the HSS waveform. The corresponding amplification for S waves at KMU starts at the lower frequency of 0.6 Hz, but it is

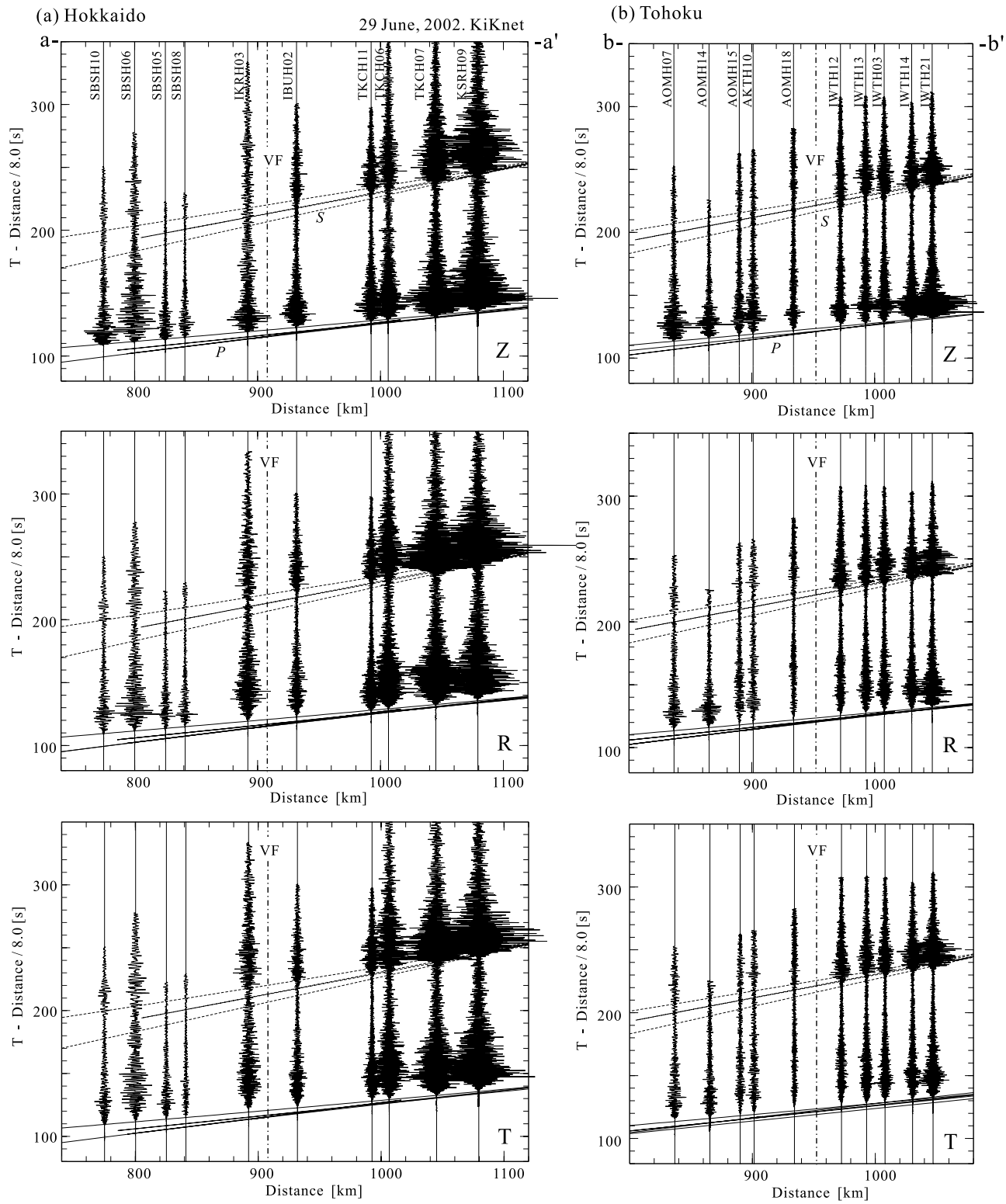

Figure 2. Three-component record section of ground acceleration from the 28 June 2002 Vladivostok event derived from KiK-net borehole stations along profiles in (a) Hokkaido and (b) Tohoku, across the volcanic front (VF), which are indicated in Figure 1c. The horizontal components have been rotated to radial (R) and tangential (T) motions relative to the path to the hypocenter. To compensate for geometrical spreading, each trace is scaled by the epicentral distance. The station names are indicated at the top of the section. VF denotes the position of the volcanic front. The travel times for the ak135 model are marked on the record sections.

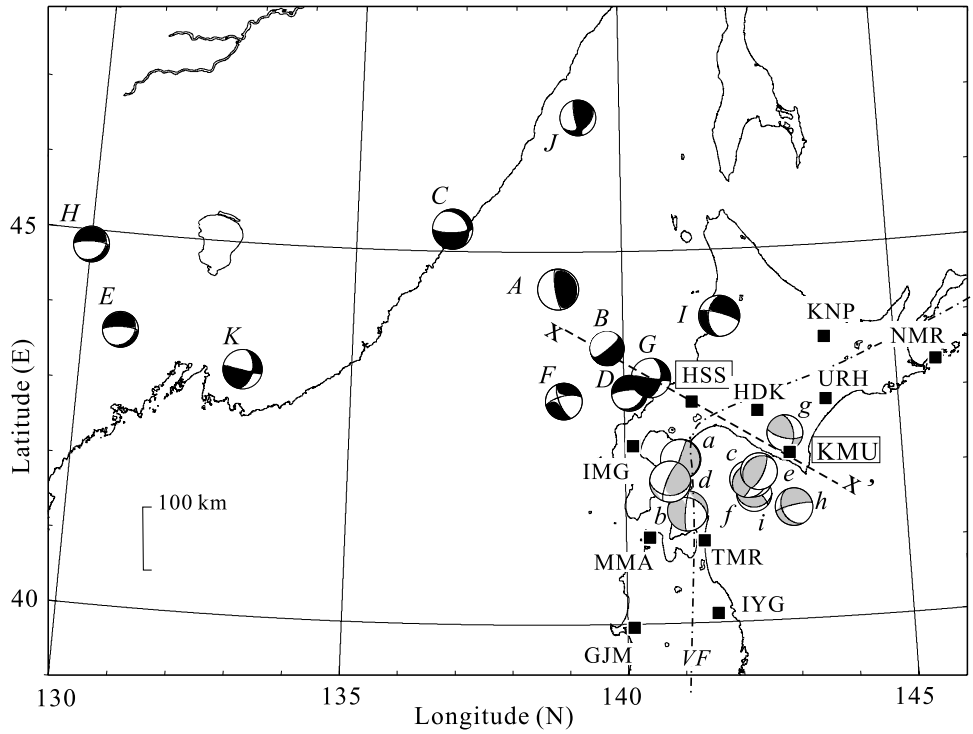

Figure 3. Stations in the FREESIA network in northern Japan and the epicenters of deep focus earthquake from April 2000 to February 2003 for which broadband observations are available. The dashed line in the middle of the Japanese islands indicates the volcanic front for Pacific subduction.

difficult to get a good estimate of the spectral ratio for *S* because of the interference of the large high-frequency *P* coda with the *S* waves. The lower frequency onset of amplification arises from the lowered *Q* for *S* waves traveling to HSS compared with the *P* waves.

3. Observations of Slab Guided Waves

[21] A consistent feature in the waveforms from deeper earthquakes in the subducting Pacific plate is that the seismograms show a low-frequency ($f < 0.25$ Hz) *P* and *S* onset followed by delayed high-frequency ($f > 2$ Hz) waves with a long coda [e.g., *Iidaka and Mizoue*, 1991; *Abers*, 2000]. This pattern seems to be a common characteristic of the waveforms from deep event in the subducted plate, such as for the Cocos plate of Nicaragua [*Abers et al.*, 2003], and the Nazca slab at the Chile-Peru subduction zones [*Isacks and Barazangi*, 1973; *Snoke et al.*, 1974; *Martin et al.*, 2003].

[22] The longer-period precursor from the deep Pacific plate events is very clear at the stations KMU, URH, NMR, TMR, and IYG, on the forearc side of the volcanic front (Figure 6). The low-frequency onset of *P* and *S* is particularly striking at KMU which has a good signal-to-noise ratio.

[23] Expanded segments of the broadband seismograms at KMU for event C are shown in Figure 7 with increased time resolution for both *P* and *S* waves and are accompanied by filtered seismograms with a corner frequency of 1 Hz. The low-frequency ($f < 0.25$ Hz) precursor which appears on both the radial (R) and vertical (Z) components represents the direct propagation of *P* waves from the source to the station along the great circle path. No clear *P* precursor appears on the transverse (T) component. The delay in the arrival of the higher-frequency ($f > 2$ Hz) signals is about 1 to 1.5 s for *P* and 1.5 to 2 s for *S* waves. The high-frequency waves sustain a large amplitude for 20 s or so and continue for a very long time on all three components. The complexity of these high-frequency arrivals suggests they represent the effect of scattering by heterogeneity.

[24] The broadband waveforms at KMU were examined for 20 recent events with a magnitude of about M_w 4.5 or larger lying to the west of the station with a variety of source depths, 44–566 km (Table 1 and Figure 3), to examine the character of the precursors as a function of varying source depth. In Figure 8 we illustrate the radial component broadband waveforms at KMU as a function of source depth for events with a similar azimuth. The low-frequency *P* onset appears at KMU when the source is deeper than 185 km, but suddenly disappears as the source approaches the surface. The delay time to the high-frequency later signal is almost unchanged with increasing source depth, and has a specific value at each station (Figure 6).

[25] Several theories have been proposed to explain the cause of such low-frequency precursors: reflection from the boundary inside of the top of the plate [*Snoke et al.*, 1974; *Iidaka and Mizoue*, 1991]; dispersion by propagation in the thin low-wave speed oceanic crust at the top of the plate [*Abers*, 2000; *Martin et al.*, 2003]; and some sort of multipath effect [*Barazangi et al.*, 1972]. However, the pronounced characteristics of large amplitude and long duration high-frequency signals in the three-component ground motion cannot be explained by the current models.

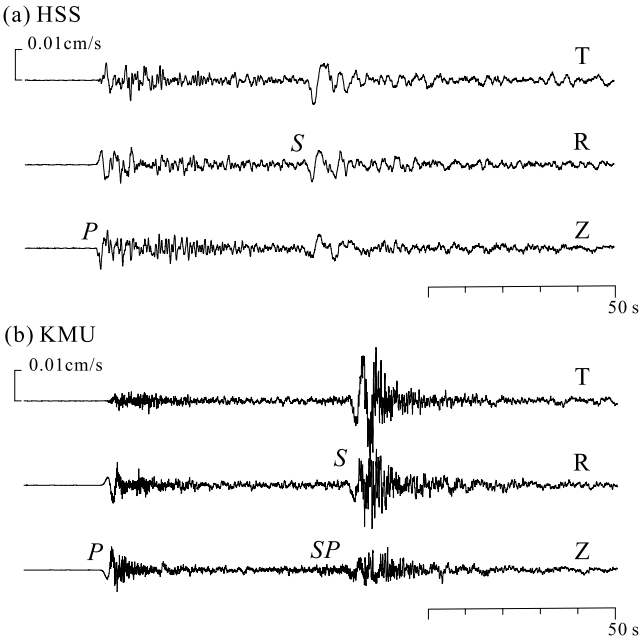

Figure 4. Three-component broadband record for the 2 February 2002 event recorded at (a) HSS in the back arc and (b) KMU in the forearc.

[26] We introduce a scattering waveguide model for the subducting plate to provide efficient trapping of high-frequency waves with wavelengths shorter than the scales of the scatterers. We will demonstrate with numerical simulations that specific forms of stochastic heterogeneity inside the plate can cause the observed separation between the low-frequency precursor and the later high-frequency signal.

4. Modeling of Slab Guided Waves

[27] We illustrate the way in which a scattering waveguide can arise in the subducted Pacific plate by conducting a suite of numerical simulations of 2-D seismic wave propagation for different styles of heterogeneous subducting plates embedded in a standard subduction model with fixed crust and upper mantle structure (Figure 9). The guided waves are built up by multiple forward scattering from the internal heterogeneity in the plate.

[28] The 2-D model is taken along a profile cutting across Hokkaido through the broadband stations HSS and KMU, nearly perpendicular to the trench, extending to the region of deep events in the Pacific plate (line x–x′ in Figure 3). For simplicity, we perform the simulation in a 2-D Cartesian coordinate system, so that the effect of spherical Earth structure and surface topography are ignored. This simplification does not have significant effects on the regional seismic wave field from a deep earthquake in the plate.

[29] The physical parameters for the crust and upper mantle structure for northern Japan are based on the ak135 reference Earth model [*Kennett et al.*, 1995], with a varying depth to the crust/mantle boundary (Moho) and the midcrustal (Conrad) interface derived from the model of *Ryoki* [1999]. The shape of upper boundary of the Pacific plate is based on the model of *Katsumata et al.* [2003]. The anelastic attenuation for *P* and *S* waves is introduced in this simulation using the damping model of *Robertsson et al.* [1994], which yields frequency-independent constant attenuation (Q_P and Q_S) for both *P* and *S* waves over a wide frequency range.

[30] The 2-D model covers a region of 400 km horizontally and 280 km in depth, discretized with a uniform grid interval of 0.06 km. We use the parallel finite difference method (FDM) in a staggered grid configuration with sixteenth-order accuracy in space and second-order accuracy in time. The higher-order FDM with a fine grid model can simulate seismic wave propagation to the relatively high-frequency of 18 Hz with sampling of 3.14 grid points per shortest wavelength for a minimum shear wave velocity of V_S = 3.4 km/s. Artificial reflections from model boundaries are suppressed by employing an absorbing damper [*Cerjan et al.*, 1985].

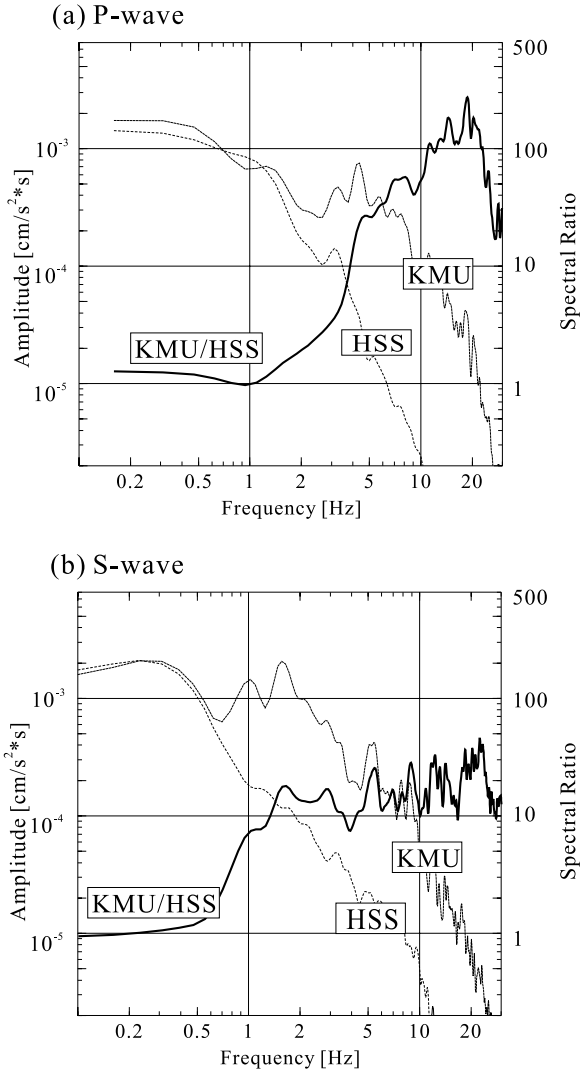

Figure 5. Fourier spectrum of the broadband records at HSS and KMU shown in Figure 4 for (a) *P* waves and (b) *S* waves and the spectral ratio of KMU relative to HSS (thick line).

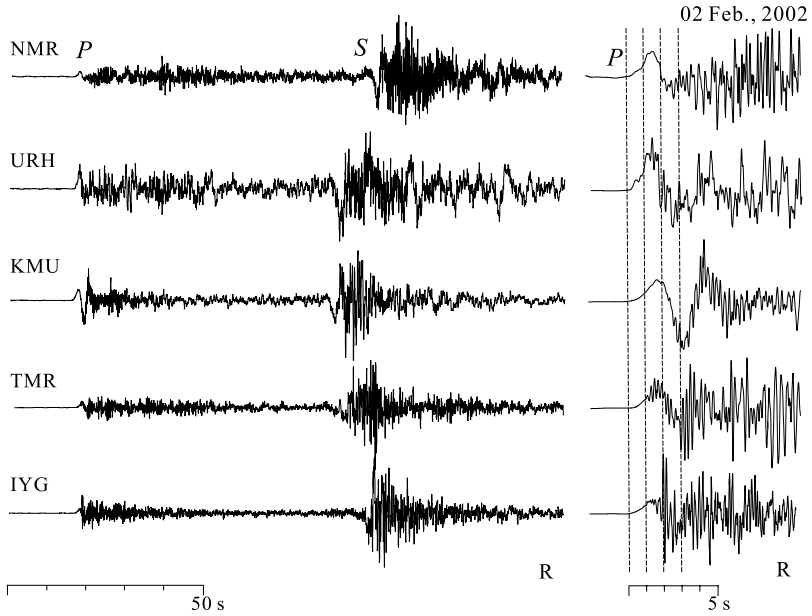

Figure 6. Radial component broadband waveforms at five stations on the forearc side for the 2 February 2002 event. An expanded *P* wave segment is displayed at the right.

[31] A double-couple line source, with normal faulting, representing the 3 December 2001 event (M_w 5.4; h = 220 km; marked as B in Figure 3) is incorporated in the plate 5 km below the plate surface. The time dependence of the seismic line source is a pseudo-delta function with radiation of seismic waves up to a maximum frequency of 18 Hz. The synthetic seismograms for the deep M_w 5.4 event, inside the plate, are obtained by convolution with the slip velocity function derived by *Nakamura and Miyatake* [2000], assuming a fault size of 1 km × 2 km, risetime of 0.15 s, rupture speed of 3.4 km/s, stress drop of 10 MPa, and a source dependent f_{max} of 10 Hz (Figure 9).

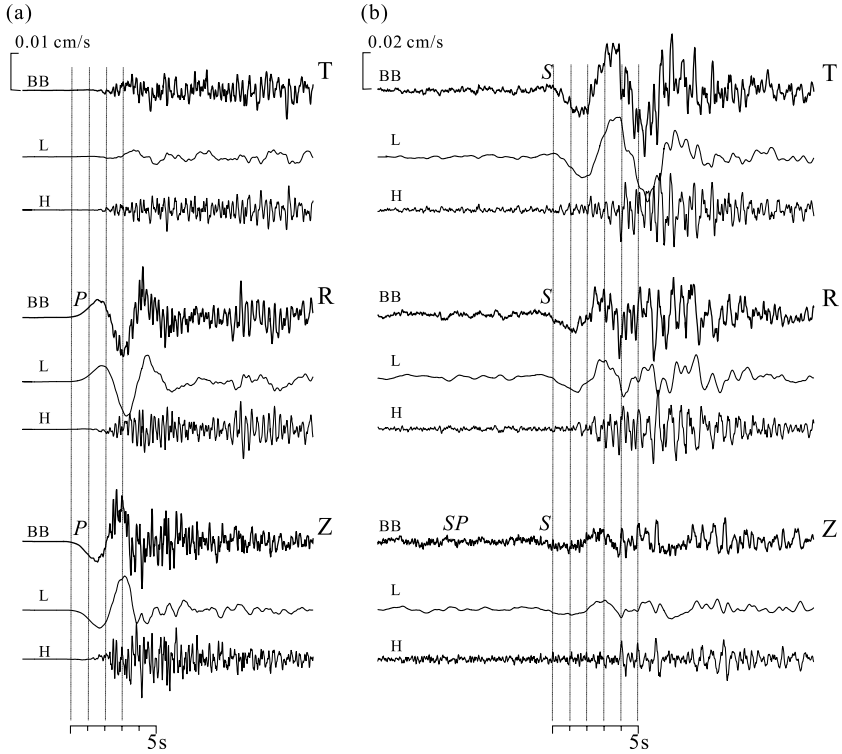

Figure 7. Segments of the three-component waveform at KMU for the earthquake shown in Figure 4 for (a) *P* and (b) *S* waves, with an unfiltered broadband record (BB), low-pass-filtered waveform with cutoff frequency at 1 Hz (L), and the waveform with a high-pass filter above 1 Hz (H).

Table 1. Epicentral Information for Events With an Identified Early Longer-Period Arrival, 1 September 2001 though 31 August 2003 Shown in Figure 3

Mark	Date	Time, UT	Latitude, °N	Longitude, °E	Depth, km	Magnitude M_w	Event Region
			Events With an Early Long-Period Arrival				
A	10 Sep 2001	2053	44.5	138.8	320	5.3	eastern Sea of Japan
B	3 Dec 2001	2334	43.7	139.7	220	5.3	NW off Shakotan peninsula
C	2 Feb 2002	2155	45.3	136.8	400	5.9	near Vladivostok
D	1 May 2002	0556	43.1	140.1	200	4.6	NW off Shakotan peninsula
E	28 Jun 2002	1719	43.7	130.7	566	6.8	eastern Russia
F	19 Jul 2002	1508	43.0	138.9	250	4.9	eastern Sea of Japan
G	28 Aug 2002	0743	43.3	140.5	185	4.5	Shiribeshi region
H	15 Sep 2002	0939	44.8	130.0	578	6.3	eastern Russia
I	19 Feb 2003	0502	44.1	141.8	240	5.9	Rumoi region
J	27 Jul 2003	0625	46.8	139.2	520	6.8	southern Siberia
K	31 Aug 2003	2308	43.3	133.0	520	6.1	near Vladivostok
			Events With No Early Longer-Period Arrival				
a	27 Apr 2000	0538	141.0	42.2	110	4.5	south off Tomakomai
b	16 Jun 2000	0736	141.1	41.5	155	4.6	Tsugaru Strait region
c	10 Jul 2002	1448	142.3	41.7	44	4.8	east off Aomori prefecture
d	29 Aug 2002	0904	142.3	41.9	62	4.8	south off Urakawa
e	23 Feb 2003	1700	142.4	42.0	47	4.9	south off Urakawa
f	8 Mar 2003	2312	140.8	41.9	110	4.5	Oshima prefecture
g	16 Mar 2003	0535	142.9	42.5	104	4.8	Hidaka Mountains region
h	20 Sep 2003	0931	143.0	41.5	50	4.7	east off Aomiri prefecture
i	13 Nov 2003	2239	142.2	41.9	62	5.0	south off Urakawa

[32] For parallel computing the 2-D model is partitioned vertically into 16 subregions with the overlap between neighboring regions assigned to many processors [*Furumura et al.*, 2001]. A message passing interface (MPI) is used for interprocessor communication with neighbor processors at each time step, in order to exchange data for the regions of overlap. The parallel simulation is conducted by using a PC cluster (Intel Xeon 2.66 GHz) connected to a Gigabit Ethernet computer network. Calculations for 150 s after source initiation with 100,000 time steps required 60 hours CPU time and a total memory of 4.8 GByte.

4.1. Base Subduction Zone Model

[33] The first simulation of wave propagation in the Pacific subduction zone employs the simple plate model illustrated in Figure 9. The thickness of the Pacific plate is

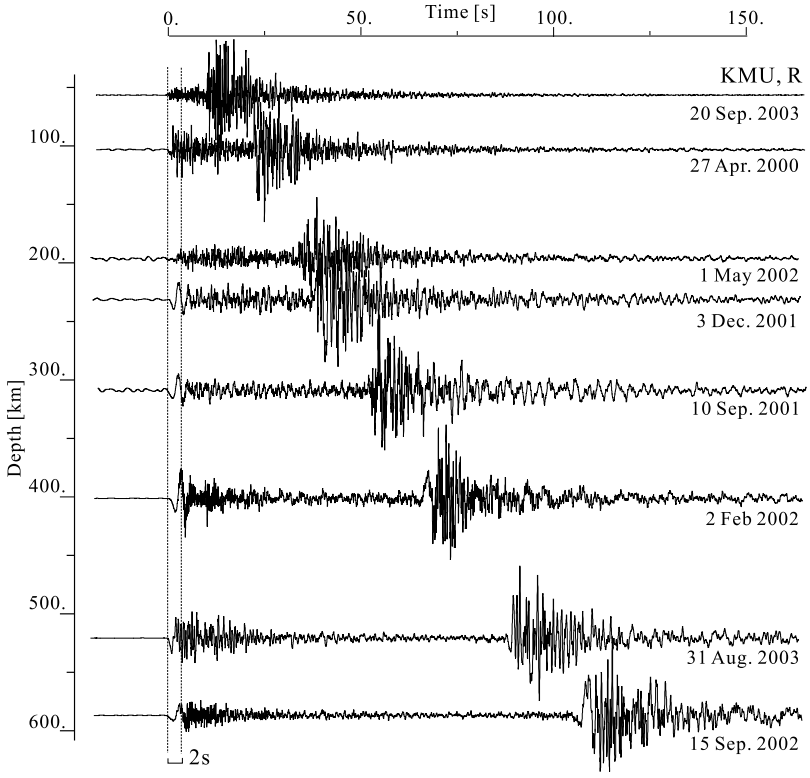

Figure 8. Comparison of radial component broadband waveforms at KMU for events with varying source depth.

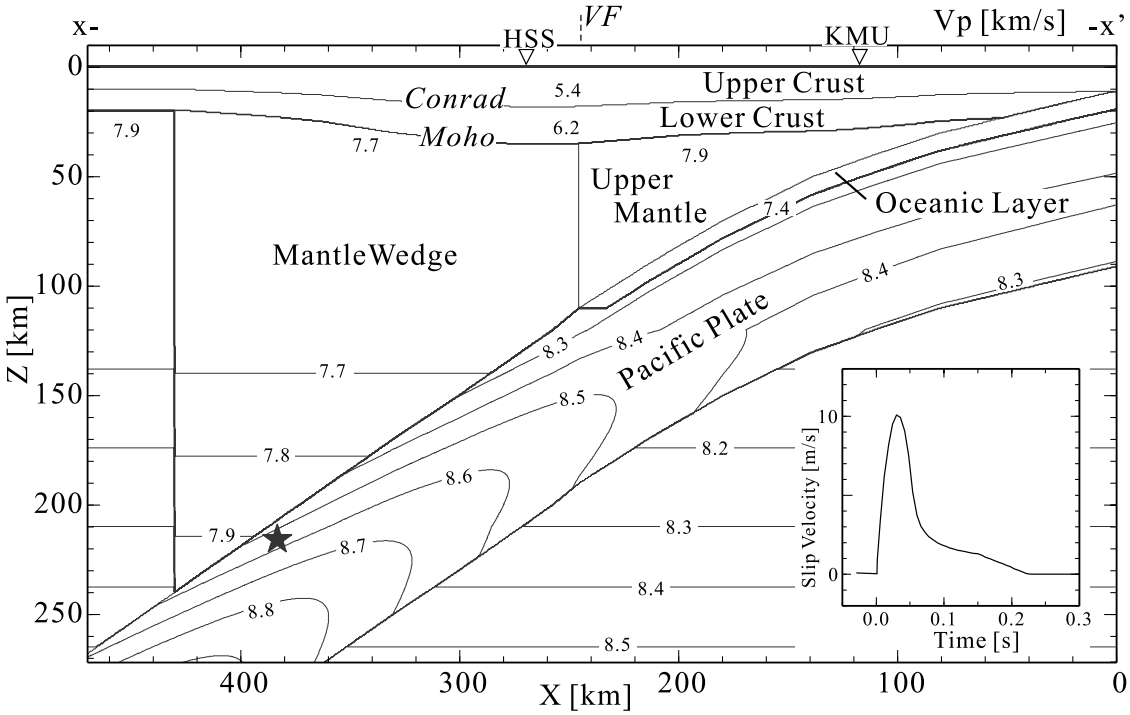

Figure 9. Depth variation of *P* wave structure used in the 2-D simulation of seismic wave propagation, along profile x–x′ shown in Figure 3. Insert shows the source time function of *Nakamura and Miyatake* [2000] for a M_w 5.4 in-slab earthquake.

80 km and a thin (8 km) layer of former oceanic crust is embedded at the top of the plate down to 110 km depth. The subducting plate has velocities and density 2% larger than the ak135 model, with in addition a small (1%) linear increase in the seismic parameters, from top to base, across the thickness of the plate. The thermal regime of the descending slab is approximated by using a 2% larger velocity and density in the center of the plate with a decrease to normal values toward either side of the plate using a cosine function.

[34] A low-wave speed zone of former oceanic crust with 8% slower velocity and density than the surrounding mantle is incorporated just below the plate surface. This zone descends with the plate to a depth of 110 km. On the basis of the studies of *Takanami et al.* [2000] and *Tsumura et al.* [2000], we assigned relatively high-Q values for *P* and *S* waves in the subducting plate (Q_P = 600, Q_S = 300) and somewhat smaller values for the oceanic crust (Q_P = 300, Q_S = 150). Stronger attenuation (Q_P = 120, Q_S = 60) is assigned to the uppermost mantle above the plate on the forearc side of the subduction zone, compared with that for the surrounding mantle (Q_P = 400, Q_S = 200).

[35] The results of the numerical simulations are shown in Figure 10 with snapshots of the seismic wave field at times 15, 30, 45 and 60 s after earthquake initiation, and waveforms of the radial and vertical components of ground velocity as a function of distance from the epicenter. Each waveform is multiplied by the square root of the hypocentral distance to provide a partial compensation for 3-D geometrical spreading from the line source.

[36] The snapshots of seismic wave field shown in Figure 10a. The simulated 2-D wave field is split into *P* (red) and *SV* (green) contributions by calculating the divergence and rotation of the wave field, respectively. In Figure 10a, the various seismic signals and the conversion between *P* and *SV* wave motions at interfaces are very clearly seen. Snapshots show that the *P* and *S* waves propagating in the high-Q and high-wave speed plate are much larger than in the surrounding mantle (see 33 s frame). The attenuation of the seismic waves traveling upward through the mantle wedge is very strong due to the passage through the low-Q zone as originally proposed by *Utsu* [1966].

[37] As the *P* and *S* waves enter the former oceanic crust, trapped waves with significant energy are built up from the superposition of multiple postcritical reflections inside the thin low-wave speed layer (indicated by O in the 30 and 45 s frames). The trapped signals travel for long distances in the thin low-wave speed waveguide from the source to trench. However, some of them escape to the crust at distances beyond about 200 km from the epicenter, due to the lower impedance contrast between the plate and mantle at that depth. The bend in the subducting plate also helps to release some energy from the trapped signals through the curved interface. Thus the amplitude of the guided *P* wave traveling in the former oceanic layer is gradually extracted to appear in the waveform at the forearc stations as the trench is approached.

[38] Record sections of synthetic seismograms for ground velocity are shown in Figure 10 with the radial component in Figure 10b and the vertical component in Figure 10c. These sections demonstrate the remarkable contrast in the shape of waveforms as the volcanic front is crossed at distance of about 150 km from the epicenter. The waveforms show intense *P* and *S* waves with dominantly high-frequency signals at stations on the forearc side. In the back arc region

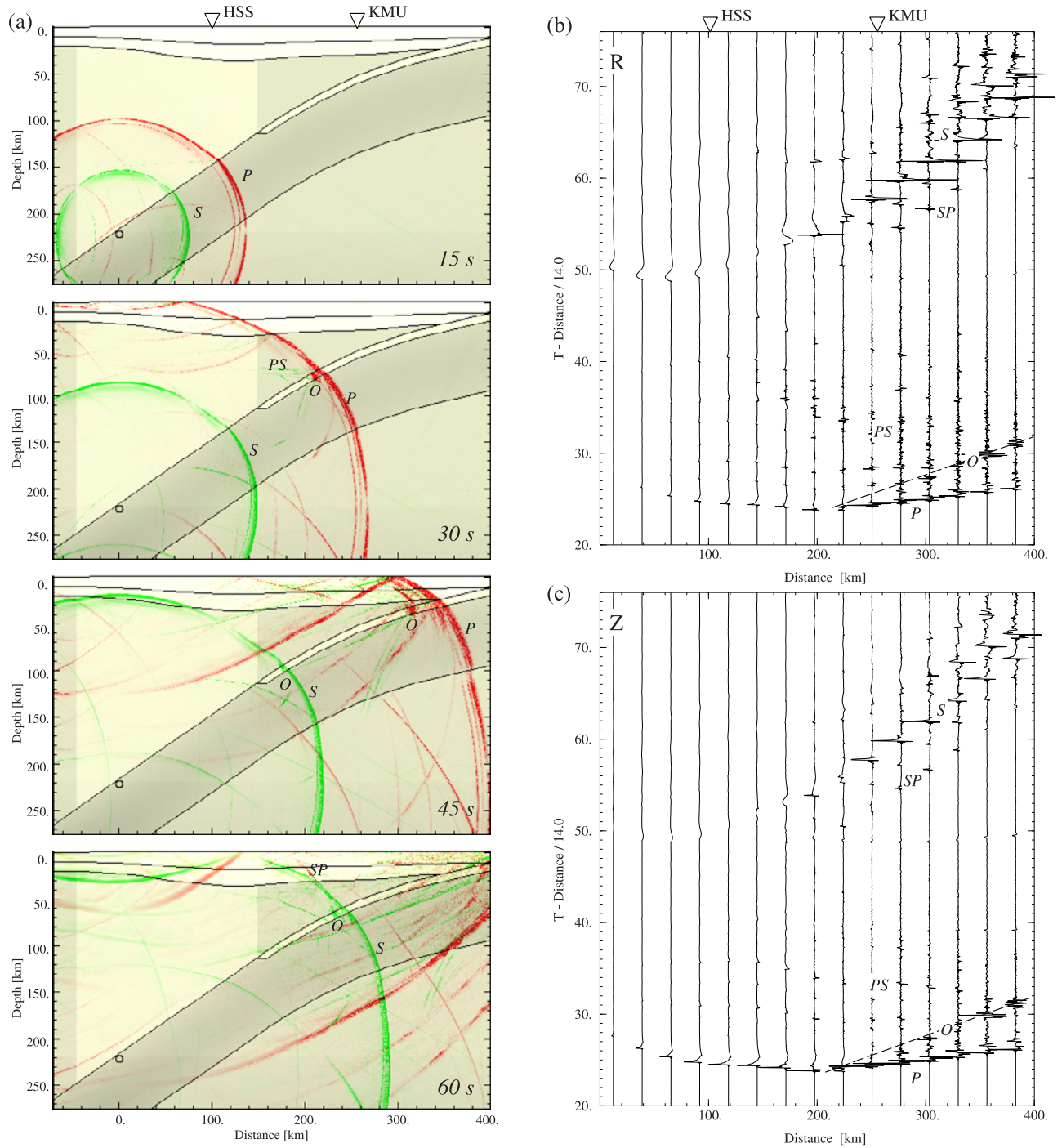

Figure 10. Snapshots of seismic wave propagation at (a) 15, 30, 45, and 60 s and the waveforms for (b) radial and (c) vertical motions derived from the 2-D simulation of propagation from subduction zone earthquake at 220 km for the base plate model of Figure 9. The contributions from the *P* waves and from *SV* waves are shown in red and green, respectively. The triangles at the top indicate the positions of the broadband stations HSS and KMU. The major seismic phases are marked. Trapped signals in the former oceanic layer are indicated by O.

the arrivals are much lower frequency because of their passage through a zone of increased attenuation (low *Q*). The loss of high-frequency signals for back arc stations is more dramatic for the *S* wave, and a small, elongated *S* wave pulse with predominant frequency less than 0.3 Hz is found similar to that in the observations at HSS (Figure 4a). Some conversions from *P*-to-*S* wave at the top of the plate (30 s frame), *S*-to-*P* conversion at the Moho interface (60 s), *S* wave reflection from the bottom of the plate (30 s), and their successive multiple reflections in the crust and upper mantle interfaces form the later arrivals of *P* and *S* waves at the forearc stations.

[39] The differences in the amplitude and frequency of waveforms between the forearc and the back arc side of the Pacific subduction zone in this simple model explain, to some degree, the large discrepancy in seismic intensity from deep plate earthquakes as the volcanic front is crossed in northern Japan (Figure 1c), and also the dramatic attenuation of *S* waves at back arc stations. However, the simulated waveforms are too simple to explain the complex observed waveforms with the very long duration of high-frequency signals at forearc stations. The *P* and *S* wave coda induced by trapping of high-frequency waves in the former oceanic layer, with lowered wave speed, is too simple and short to explain the observations at, e.g., KMU (Figure 4b).

4.2. Trapped Waves in Extended Former Oceanic Crust

[40] As a possible means of extending the *P* and *S* wave coda we modify the structural model for the plate by extending the zone of former oceanic crust to 240 km depth; to enhances the wave trapping effect in the low-wave speed layer.

[41] The source now sits in the waveguide at the plate surface so that the coupling is strong, resulting in large amplitude seismic waves in the oceanic layer in all the snapshots (Figure 11). The trapping of seismic energy is more striking for the *P* wave because the normal fault internal source radiates large *P* wave energy inside the layer. The rather weak *P* waves radiating into the oceanic mantle, also enhance the visibility of the trapped signals in the oceanic layer. On the other hand, the trapped *S* wave signal has limited expression in the seismograms. The configuration of the source is less favorable than for *P* and the larger intrinsic attenuation in the oceanic layer becomes important.

[42] As the trapped waves approach the volcanic front, the bend in the subducted plate gradually separates the trapped signal from the direct *P* wave (30 s frame). The effect of the bend in the slab to decouple the guided wave train from the oceanic crust has been also discussed by *Martin et al.* [2003]. In the seismograms for radial and vertical motion we see the development of large trapped *P* wave signals with a significant increase in amplitude as the trench is approached. Small amplitudes for the direct *P* wave also enhance the larger trapped signal.

[43] The trapped *P* phase in the thin low-wave speed layer shows remarkable dispersion characteristics in the seismograms, with faster propagation of the low-frequency signals and a following high-frequency arrival, notably for larger epicentral distances (>300 km). The simulated waveform of the faster low-frequency phase and the later, large, high-frequency signals for a near trench station has some resemblance to the observations at KMU, but does not put the low-frequency arrivals as the onset of the record. The pattern of arrivals for *S* is a set of discrete pulses rather than the continuous high-frequency arrivals seen at KMU. From a range of simulations we find that *S* waves are more easily trapped and dispersed when a thinner oceanic crustal segment (<4 km) is employed. Nevertheless it is very difficult to trap a large amount of seismic energy in such thinner crust to produce a large and long high-frequency *S* wave coda.

[44] Thus the effects of the waveguide in the former oceanic layer, with low-wave speed, provides an interesting example of a dispersed seismic wave train with a low-frequency start followed by high frequency signals. However, the extended waveguide is not sufficient to explain the observed characteristics for the deep earthquakes in the plate, at least for the Pacific subduction zone.

4.3. Effect of Random Scatterers in the Subducted Plate

[45] As an alternative mechanism for the guiding of high-frequency seismic waves in the plate we consider the influence of internal heterogeneity. This scattering waveguide model is based on the idea that small-scale heterogeneity exists in the subducting plate, and so high-frequency signals can survive within the structure due to strong multiple internal scattering. Such small-scale heterogeneities in the crust appear to be the major cause of long *P* and *S* wave coda [e.g., *Aki and Chouet*, 1975; *Frankel and Clayton*, 1984], and so we expect a similar mechanism can apply in the subducting plate.

[46] Plate heterogeneity is introduced into the former oceanic crust and oceanic mantle through an isotropic random fluctuation in the *P* and *S* wave velocities and density following a von Karmann distribution function with a relatively short correlation distance of 2 km for both the downdip direction and the thickness of the subducting plate. A 2% standard deviation of fluctuations is imposed on the base model.

[47] The stochastic fluctuations were implemented in the wave number domain by applying a wave number filter to a sequence of random numbers following the procedure of *Frankel* [1989], and the result is transformed to the physical domain by using a Fast Fourier Transform. The scale of heterogeneities in the plate is selected to produce strong seismic scattering for *P* and *S* waves for frequencies over 2 Hz, with averaged *P* and *S* wave speed in the oceanic mantle of about V_P = 8 km/s and V_S = 4.6 km/s, and corresponding wave numbers for *P* and *S* waves of $k_P \sim 1.6$ km^{-1} and $k_S \sim 2.7$ km^{-1}.

[48] The change in the high-frequency seismic wave field in the subduction zone by introducing small-scale heterogeneities in the plate is quite evident in the snapshots of the seismic wave field and synthetic seismograms, especially for *S* waves (Figure 12). A significant distortion of the *P* and *S* wave fronts traveling through the heterogeneous plate is clearly seen in the snapshots as a result of multiple internal scattering of *P* and *S* waves. By examining the split of the wave field into *P* and *SV* wave contributions, it is clear that the scattered wave field is mainly composed of *P*-to-*P* and *S*-to-*S* scattering, and the conversion of energy between *P* and *SV* waves is a much weaker effect.

[49] The concentration of the *P* and *S* wave energy at the wave front gradually decreases through repeated reflections between scatterers, so that there is a band of *P* and *S* wave energy traveling upward in the plate with rather long tails. The effect of the random heterogeneity is to produce high-frequency ground oscillations of large amplitude and long duration at stations toward the forearc side. Some of the scattered high-frequency waves also emerge from the plate to appear in the waveforms of back arc stations near the volcanic front.

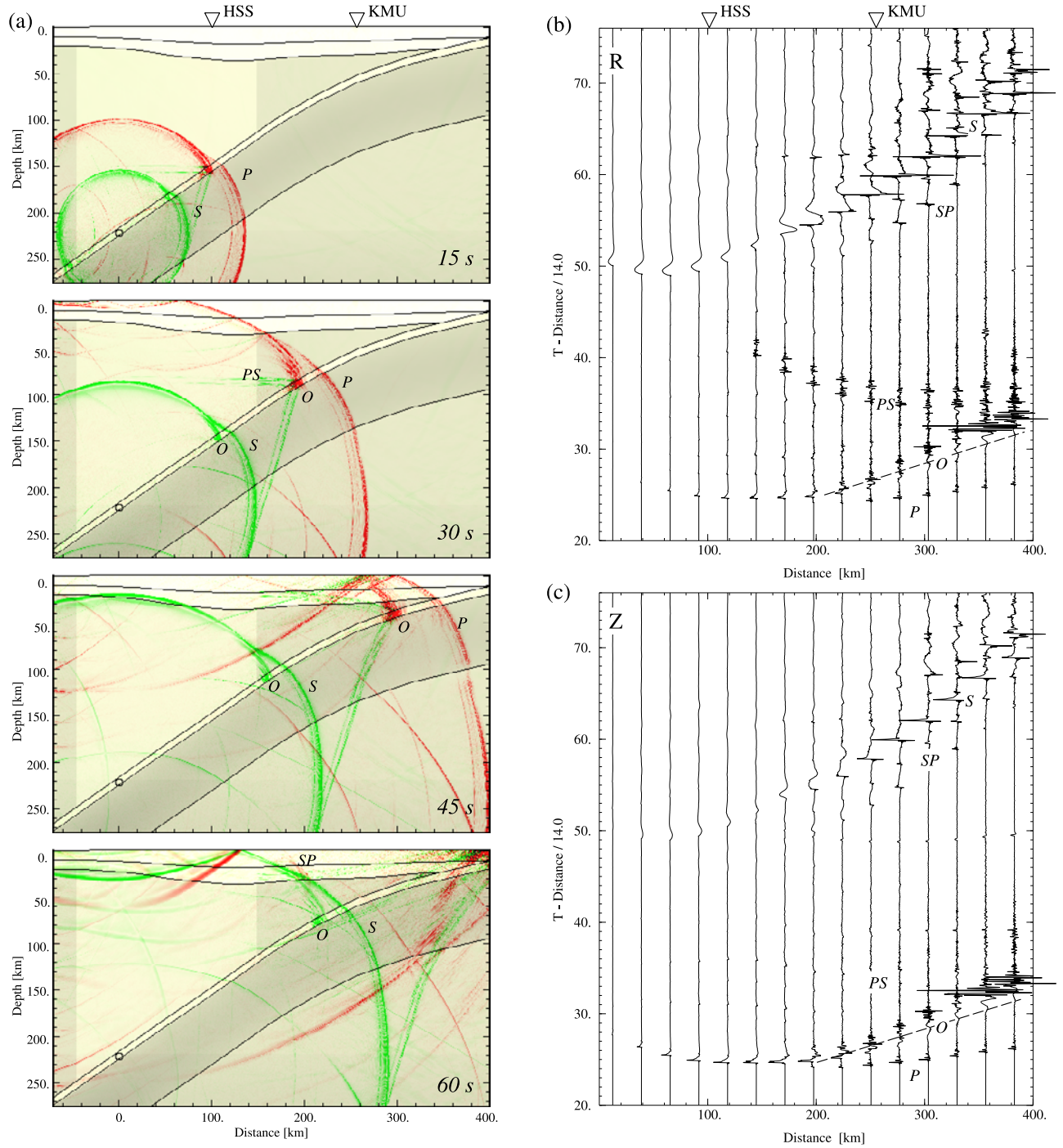

Figure 11. Same as Figure 10 but with the former oceanic crust layer descending deeper to provide a longer low-wave speed zone at the top of the plate. The seismic source is now located inside the oceanic layer.

[50] The introduction of stochastic heterogeneity leads to a significant improvement in the duration of high-frequency *P* and *S* wave coda for deep plate earthquakes, that now lasts for several tens of seconds at the forearc stations. The converted reflections from *S*-to-*P* and *P*-to-*S* are relatively small for the scattered, incoherent wave front and are therefore much less prominent than in the earlier model. The behavior appears to be closer the patterns seen in the observed seismograms.

[51] However, the simulation results for isotropic heterogeneity cannot explain the separation of the low- and high-frequency components of the signals for both *P* and *S*. which is also an important feature of the observations of the deep subduction zone earthquakes. As can be seen in the snapshot sequence in Figure 12, the leakage of high-frequency energy into the upper mantle from the high-wave speed plate is very strong. Thus this model of isotropic stochastic heterogeneity in the subducted plate is insuffi-

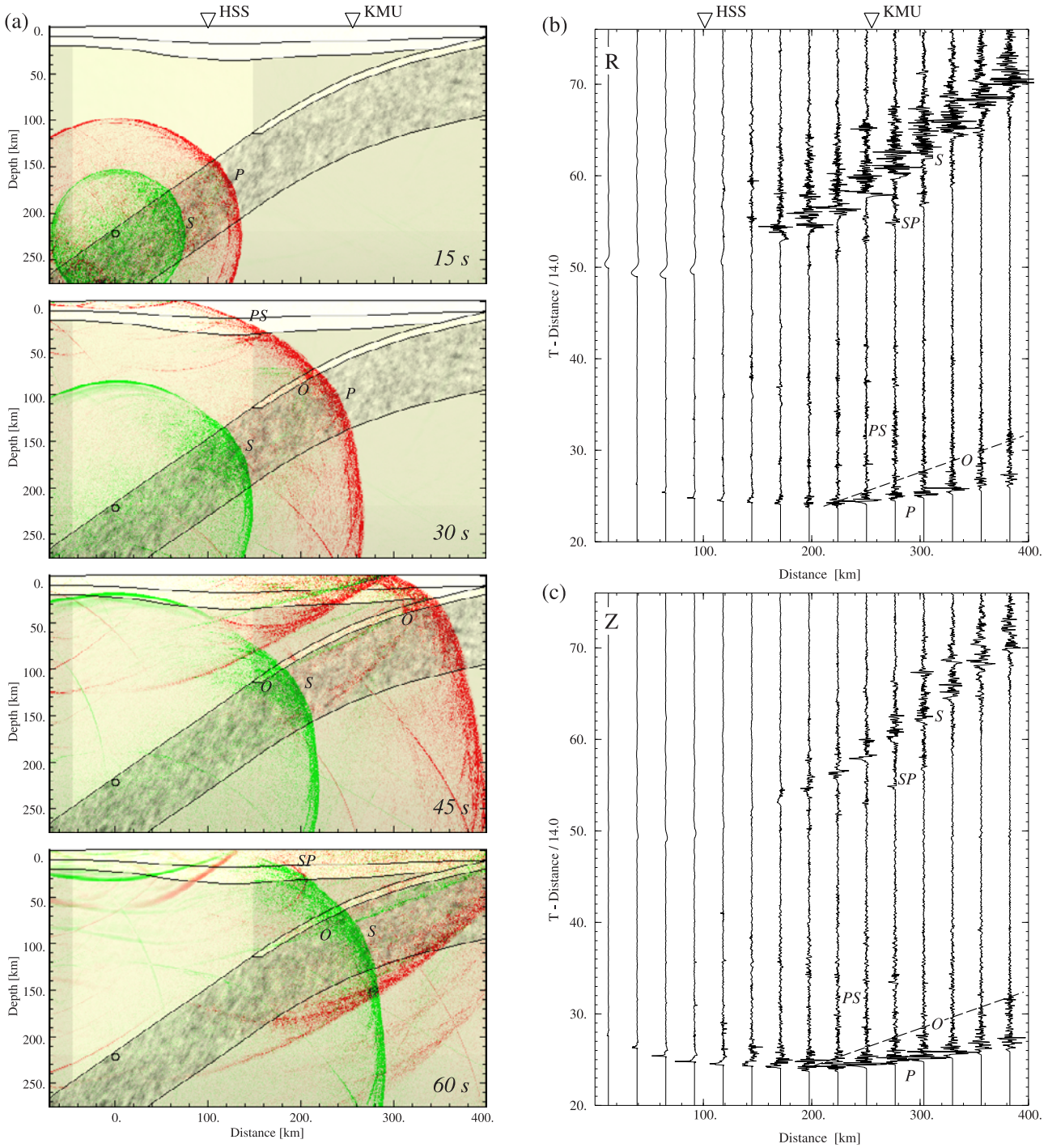

Figure 12. Same as Figure 10 but for random plate model with an isotropic velocity fluctuation described by the von Karmann function with a correlation length of 2 km and standard deviation to the average background model of 2%. The same random fluctuation in elastic properties are assigned in the former oceanic crust and oceanic mantle, but the fluctuations in the crustal segment are not displayed so as to improve the visibility of weak signals in the crust.

cient to match the required characteristics of the observations, in particular the anomalously large intensity at stations near the trench from deep, distant earthquakes.

4.4. Elongated Scatterers in the Plate

[52] To improve the match to the pattern of observations, we modify the shape of the random heterogeneities in the plate to keep high-frequency energy trapped in the plate. The new heterogeneous model includes an anisotropic form of stochastic distribution described by an ellipsoidal correlation function with elongation in the correlation distances in the downdip direction for the plate and a much shorter correlation distance in thickness. Figure 13a shows an example of such laminated plate structure

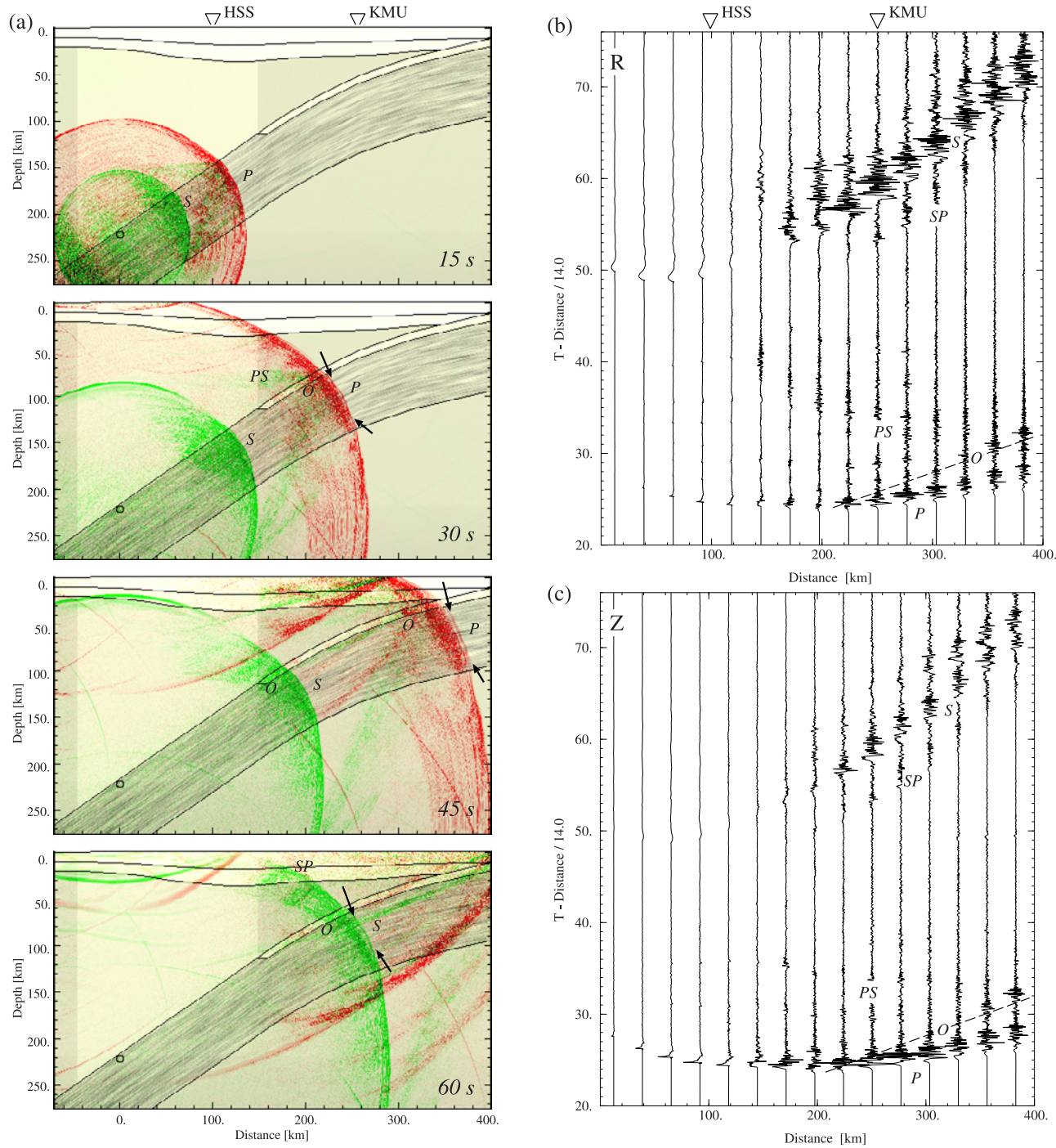

Figure 13. Same as Figure 12 but for the random plate model with horizontally extended random fluctuations with a longer correlation length of 10 km in the downdip direction and 0.5 km in thickness and a standard deviation of elastic constants from the average background model of 2%. Arrows in the snapshots indicate the tunneling of low-frequency *P* and *S* waves from the scattering waveguide.

described by the von Karmann function with a correlation distance of 10 km downdip and a shorter correlation distance of 0.5 km in thickness. The standard deviation of seismic parameters is 2% as in the previous model (Figure 12).

[53] The inclusion of the elongated random scatterers in the plate produces a strong waveguide effect for high-frequency *P* and *S* waves with enhanced forward scattering within the plate arising successive postcritical reflections at the surfaces of the lamellae. This leads to a large concentration of seismic *P* and *S* wave energy in the center of the plate and thus the seismic waves can travel longer distances along the plate with only limited loss compared to the previous experiments for the homogeneous plate and the heterogeneous plate including isotropic random scatterers. The leakage of seismic

energy from the high wave speed plate is much lower for the new plate model, as can be seen by comparison between the snapshot frame at 30 s for *P* waves and 60 s for *S* waves with the results for the previous experiment (Figure 12).

[54] The waveforms from the 2-D numerical simulations with anisotropic random scatterer in the plate show a separation of the low-frequency *P* and *S* onset and later high-frequency signal comparable to the observations at KMU (Figures 7 and 4). The snapshots in Figure 13a show the development of the separation of the frequency components for the *P* and *S* waves traveling in the plate. The multiple postcritical reflections of high-frequency signals from the heterogeneous structure within the plate cause variations in the effective wave speed for high-frequency signals which are accompanied by a long coda. However, low-frequency waves can easily pass through such small heterogeneities at faster propagation speed as like an inhomogeneous wave [*Ikelle et al.*, 1993] or as a "tunneling wave" [*Fuchs and Schulz*, 1976], with rapid wave front healing. The result is frequency-selective wave propagation in the scattering waveguide with a faster low-frequency signal and a later, large high-frequency signal with a very long coda. The trapping of the high-frequency signals in the heterogeneous plate is more efficient for *S* waves, because no conversion to *P* occurs for post-critical *S* wave reflections. For the same reason, the tunneling of the low-frequency *S* wave signal should also be more important; this is clearly confirmed in the snapshots in the last frame (60 s), but is not easily seen in the synthetic seismograms because of the influence of the coda of *SP*.

[55] The offset time between the *P* onset and the later major high-frequency signal in the simulated seismograms is about 1 s for the position of the station KMU, which corresponds very well to the observations at this station. We find from the snapshots that the bend of the subducted plate below the volcanic front helps to separate the low- and high-frequency signals, so that the synthetic seismograms show increasing time separation with increasing distance from the volcanic front in accord with the observations at forearc stations (Figure 8).

4.5. Effect of Removing the Former Oceanic Crust Component

[56] In order to clarify the importance of the thin, low-wave speed former oceanic crust on the guiding of high-frequency *P* and *S* wave signals, we finally show an example of simulation using the same random plate model shown above (Figure 13) but the oceanic crust removed from the top of the plate (Figure 14).

[57] Even in the random plate model without the former oceanic crust, the prominent character of the slab guided signals with a long high-frequency coda and separation of high- and low-frequency signals still appear in the snapshots and synthetic seismograms, except for some trapped signals in the oceanic crust (marked by '*O*' in Figures 10–13). The results of the simulations indicate that the former oceanic crust at the top of the plate can act as a waveguide for high-frequency signals and can somewhat extend the duration of *P* and *S* wave coda, but it is not a main cause of large and very long *P* and *S* wave coda to produce anomalously large intensity, and the separation of low- and high-frequency signals.

4.6. Influence of the Shape of Random Heterogeneities on the Regional Wave Field

[58] We have conducted a set of additional simulation experiments to examine how the character of the stochastic heterogeneity in the plate influences the trapping of the high-frequency seismic wave field. The correlation properties and the amplitude of heterogeneity have been varied between the different plate models.

4.6.1. Aspect Ratio

[59] The aim of the first set of experiments is to see how the shape of random scatterers in the plate affects the development of the high-frequency coda and the separation of low- and high-frequency signals. We consider four stochastic media sharing identical statistics of the elastic parameter distributions (standard deviations of 2%) and area of scatterers (roughly 2×2 km^2), but with a varying aspect ratio of the correlation function for the heterogeneities of 1, 5, 20, and 80 between the downdip direction and the thickness.

[60] Synthetic seismograms of radial ground velocity motions for a source at a fixed epicentral distance of 254 km from KMU are compared in Figure 15a. Isotropic scatterers in the plate (aspect ratio of 1) produce strong scattering of high-frequency signals and so a very long coda in *S* waves (Figure 15a, curve a). As we have seen earlier (Figure 12), the leakage of high-frequency energy from the heterogeneous plate to the upper mantle is very strong, and produces significant attenuation of the seismic waves with time.

[61] As the aspect ratio of the random scatterer increases, the length of the *S* wave coda and the peak amplitude of the *P* and *S* waves decrease gradually (Figure 15a, curves b–d). This is because the extended scatterers prevent the seismic energy from escaping out of the random waveguide in the plate, and so the amplitudes at the surface station (KMU) are weakened somewhat.

[62] On the other hand, we find a clear development of the separation of the low-frequency *P* and *S* wave onsets from the main high-frequency signals with increasing aspect ratio of the random scatterers (Figure 15a, curves b–d). The elongated scatterers with both lowered and raised wave speed variations can easily produce postcritical reflections at nearly flat interfaces, and allow penetration of low-frequency signals as an inhomogeneous wave.

[63] The random plate model we used in the previous experiment (Figure 13) with a correlation distance in downdip direction of 10 km and in thickness of 0.5 km (aspect ratio of 20), corresponds to the waveform in Figure 15a (curve c), and is able to produce both relatively large arrivals of the high-frequency signals at forearc stations and a clear separation of the low and high frequencies of *P* and *S* wave signals with long codas.

4.6.2. Standard Deviation

[64] We also examined the change in the waveforms as the level of random fluctuations is varied in models sharing the same elastic properties. We use the model of Figure 13 for which the seismogram at KMU is displayed in Figure 15a (curve c) with a common source receiver configuration. The level of the random fluctua-

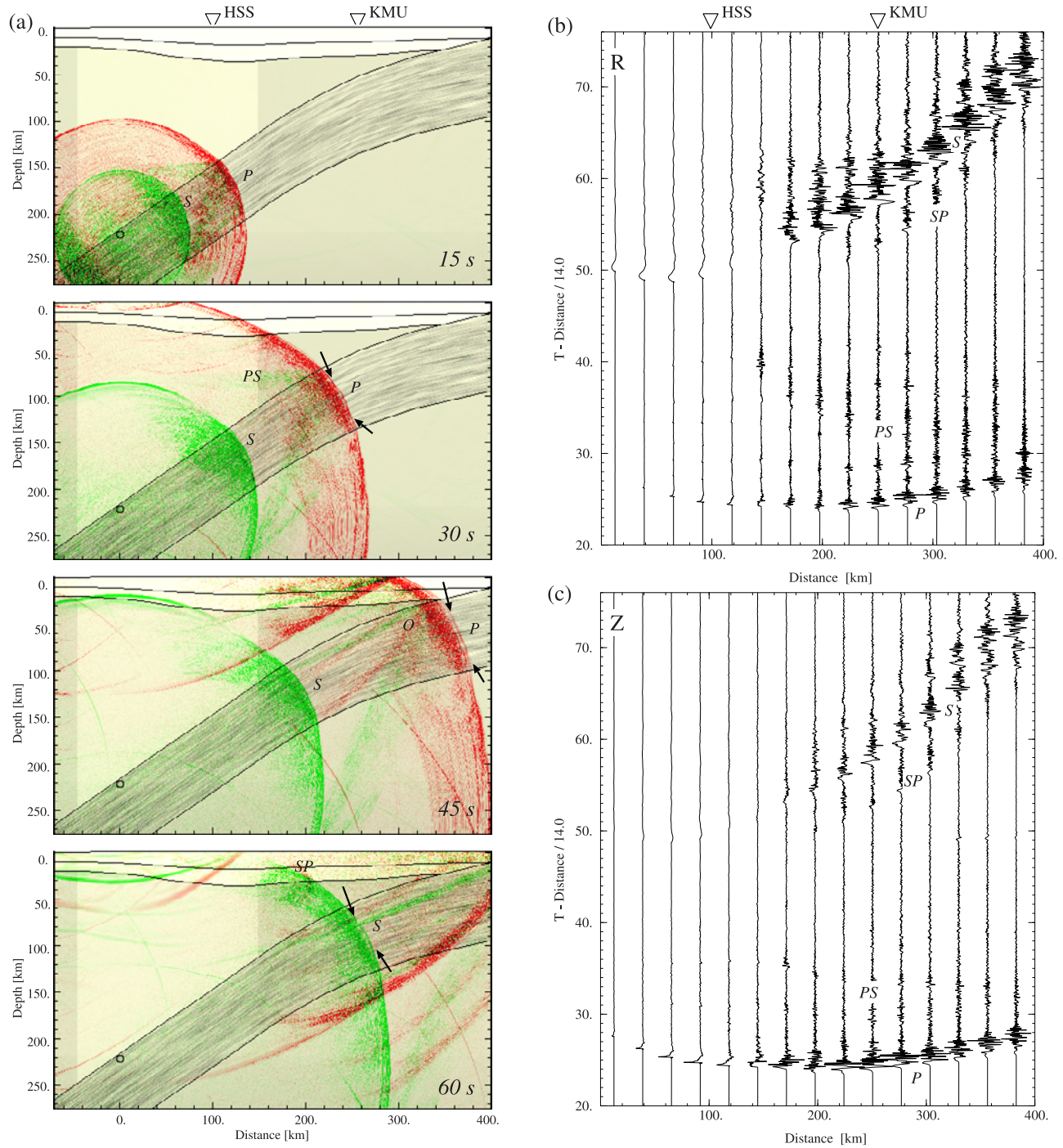

Figure 14. Same as Figure 13 but excluding the low-wave speed former oceanic crust layer from the plate model.

tions is set at 1, 2, 4, and 8% of the average background model.

[65] The resulting seismograms at KMU are shown in Figure 15b, because we are dealing with the superpositions of waves with multiple scattering paths there is no simple linear relation to the amplitude of the anomalies. Larger random fluctuations in elastic parameters extend the onsets of the *P* and *S* wave arrivals, and enhance the length of high-frequency *P* and *S* wave coda. With a very large fluctuation in random heterogeneity (8%) the onsets of *P* and *S* are rather vague with an emergent *P* onset and long coda of *P* and *S* waves (Figure 15b, curve d).

[66] Larger deviations in elastic constants increase the separation between the faster low-frequency *P* onset and the later high-frequency signals, with a nearly linear increase in the offset time from about 0.5 to 4 s with increasing fluctuation deviation from 1 to 8% (Figure 15b, curves a–d). Thus the separation time observed at KMU (about 1 to 1.5s for *P* waves) would be roughly explained by a heterogeneous model with a standard deviation of 2% as

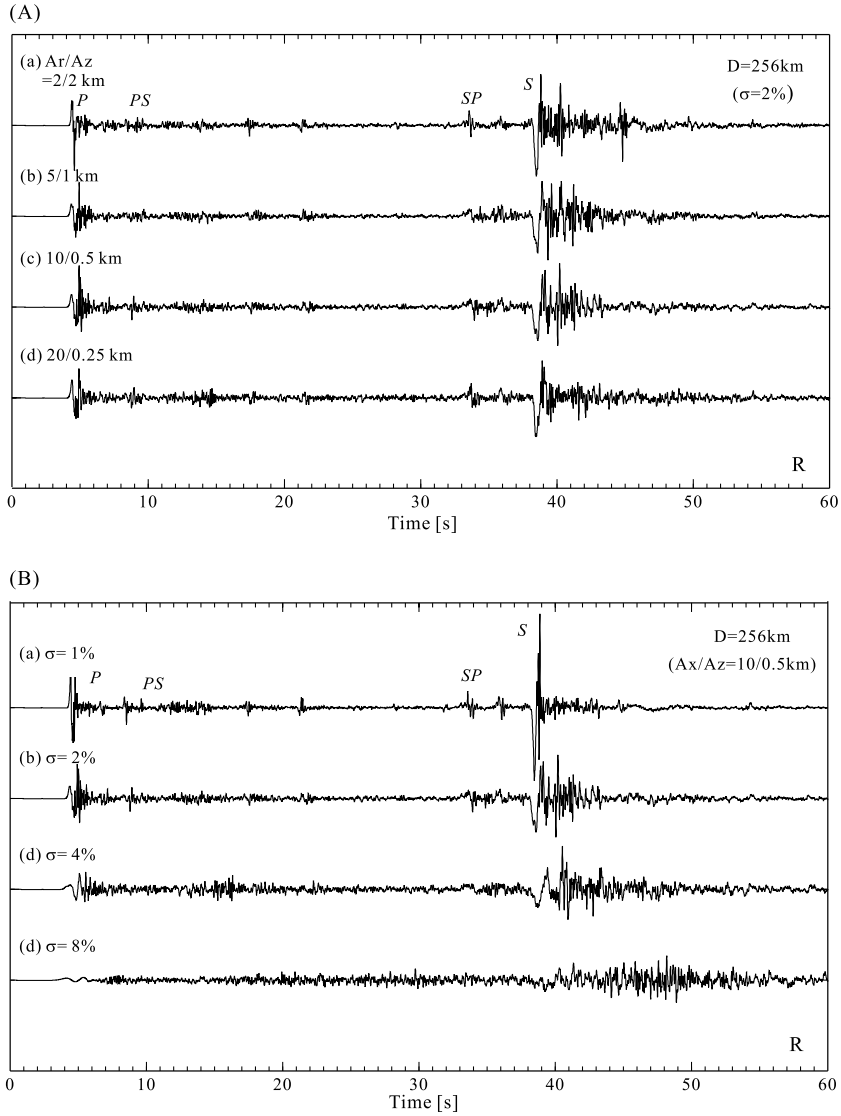

Figure 15. Synthetic seismograms from different classes of random heterogeneities inside the plate for random structure with (a) different ratios of correlation length in the downdip direction to thickness and the same standard deviation (2%) of fluctuations, and (b) different levels of random heterogeneity and the same random fluctuations in elastic constants with a correlation length of 10 km downdip and 0.5 km in thickness.

shown earlier (Figure 13 with the corresponding waveform in Figure 15b, curve c).

[67] Our results are for a 2-D model and thus account only for the scattering effects in the in-plane (x−z) direction, and miss out-of-plane scattering. We have taken a relatively simple model and have not attempted to include further small-scale heterogeneity in the crust near the stations. We may need to modify the conclusions on the nature of the stochastic heterogeneity for full 3-D scattering somewhat, but at present cannot carry the calculations to very high frequencies. We can reproduce the main features of the observed seismograms, but cannot expect a detailed match with the simplified model.

4.7. Influence of Plate Heterogeneities With Varying Source Depth

[68] Our simulations have so far employed a fixed source in the subducted plate at depth 220 km. However, the characteristics of frequency-selective wave propagation from the subduction zone earthquakes we discussed above appears for all events deeper than 185 km in the Pacific plate.

[69] To see how the characteristics of the seismograms depend on source position we have performed a set of numerical experiments with the subduction zone model with elongated scatterers (Figure 13). We use the seismic reciprocal theorem to construct, in a single calculation, a set of waveforms for a single receiver at KMU corresponding to many different source positions.

[70] Synthetic seismograms from this reciprocal calculation are displayed in Figure 16a for a set of sources set 5 km below the top of the plate at epicentral distances to KMU varying from 0 to 360 km. The set of reciprocal seismograms for radial component motion (Figure 16a) shows relatively long *P* and *S* wave codas built up from multiple scattering in the heterogeneous plate. Enhanced attenuation of the *S* wave coda occurs for epicentral distances beyond

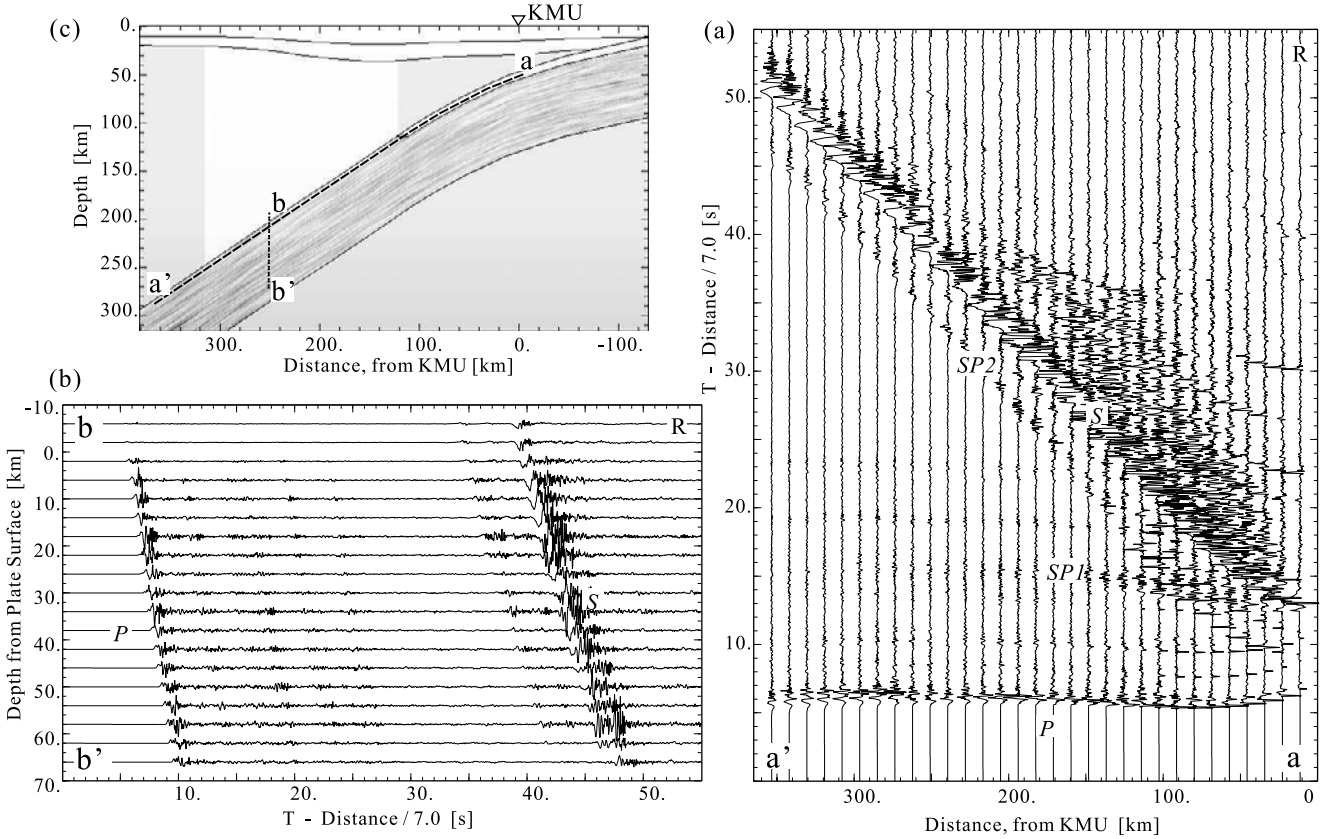

Figure 16. Reciprocal seismograms calculation for a receiver at KMU. The radial component seismograms show the evolution of the regional waveforms for a deep plate event with a double couple source at (a) the descending plate 5 km below the plate surface and (b) at a fixed distance of 254 km from KMU and source depth of −10 to 70 km from the plate surface. (c) Configuration of sources and stations for the reciprocal calculation.

110 km as the signals travel through the low-Q mantle wedge once the source position lies on the back arc side of the volcanic front.

[71] The separation of the low-frequency onset from the later high-frequency component in the simulations is distinct for events with epicentral distances to KMU of over 200 km, which corresponds to the source depth deeper than 180 km. There is therefore a close correspondence with the observation that the separation of the low-frequency P onset at KMU arises only for events deeper than 185 km (Figure 8). The delay of the second high-frequency signal following the low-frequency P onset is gently enhanced with increasing epicentral distances. The maximum separation of about 1.5 s for P wave and 2 s for S wave also agrees well with the observation at KMU (Figure 7), though the increase in the separation time with epicentral distance is not so apparent in the observations (Figure 8). This may reflect a modification of the heterogeneity structure in the deeper part of the subducting plate.

[72] While the source lies within the low-wave speed zone of the former oceanic crust, at depth below 110 km (distances less than 110 km to KMU), a strong enhancement in trapped S phases is seen in the synthetic seismograms. A relatively large S-to-P conversion occurs at the interface of the low-wave speed layer and the top of the plate (marked SP1 in Figure 16a) when the source lies inside the layer. This supports the claims of *Matzuzawa et al.* [1987] based on the observation of the S-to-P conversions at the Pacific plate of northern Japan, that the descending former oceanic crust does not persist to depths greater than about 110–160 km.

[73] We also show seismograms for a set of sources at a fixed epicentral distance of 254 km to KMU with a depth range of −10 to 70 km from the upper surface of the plate (Figure 16b). The separation of the high-frequency signal from the low-frequency P onset is influenced by the location of the source relative top of the plate. The low-frequency onset is most distinct when the source lies in the upper part of the subducting plate within 40 km from the plate surface. The amplitude of the low-frequency onset then gradually decreases with increasing depth below the center of the plate. This effect arises because the tunneling of the low-frequency inhomogeneous waves occurs for a relatively narrow zone on the wave front, within the critical angle defined by the ratio of lower to higher velocities in the random heterogeneities. Thus leakage of the inhomogeneous waves from the subducting plate can easily occur when the source is close to the plate margin. When the random plate has much larger fluctuation in elastic parameters, there is a wider range for the critical reflections of scattered waves and the waveforms are much less sensitive to varying source depth.

[74] For sources near the top of the plate, the coda for *P* and *S* waves tends to be both larger and longer in duration compared to that for sources further into the subducted slab. These results suggest that we can use the observations of the nature of low-frequency *P* and *S* wave onsets and the length of high-frequency coda to provide a rough estimation of relative source location and depth in the plate.

5. Three-Dimensional Simulation of Anomalous Intensities

[75] We have so far considered seismic wave field simulation for 2-D structures on a cross section across Hokkaido, incorporating stochastic heterogeneity into the subducted plate. With a sacrifice in the resolution of the structural model and the frequency content we are able to consider 3-D seismic wave propagation from subduction zone earthquakes in a realistic model for the configuration of the Pacific plate and examine the resulting complex patterns of seismic intensity over the central Japanese archipelago.

[76] The 3-D calculations are carried out for the 12 November 2003 event (M_w 6.4; h = 360 km, Figure 1b) which occurred in the Pacific plate to the southeast of the Kii Peninsula. This deep event produced a zone of anomalous seismic intensity well away from the hypocentral area. The large intensities cover a wide area extending from Tokyo to Hokkaido along the Pacific seaboard of Japan for several hundred kilometers (Figure 1b).

5.1. Simulation Model

[77] The 3-D model for central Japan covers a zone of 512 km by 1024 km by 480 km in depth, which has been discretized with a uniform grid increment of 0.5 km by 0.5 km by 0.25 km into a 4×10^9 grid point model. Artificial reflections from the boundaries of the model are suppressed by using an absorbing boundary condition based on the perfect matched layer [*Marcinkovich and Olsen*, 2003], which is introduced in a zone of 20 grid points wide surrounding the 3-D model.

[78] The structure for the crust and upper mantle is derived from the same data set used in the 2-D simulation, including the structure of the 80 km thick subducting Pacific plate [*Zhao and Hasegawa*, 1993] and the 20 km thick Philippine sea plate [*Yamazaki and Ooida*, 1985]. Both have a 8 km thick layer of low-wave speed former oceanic layer at the top of the plate. We introduce stochastic heterogeneity throughout the former oceanic crust and oceanic mantle of the Pacific plate with a correlation length of 10 km in both the downdip and the strike direction along the plate and a much shorter correlation length of 0.5 km in thickness. The standard deviation of the fluctuations is 2% from the ak135 background model. We also assigned the similar random fluctuations to the Philippine sea plate, but the effect of random heterogeneities in the thinner (20 km) plate should be too small to cause noticeable scattering of seismic waves arriving from the source outside this plate.

[79] The equations of motions in 3-D are discretized using a accurate 32th-order staggered grid central finite difference scheme in the horizontal directions and a conventional fourth-order scheme in the vertical direction. With a minimum shear wave velocity of 3.4 km/s in the shallowmost layer and a grid size of 0.5 km in the higher-order finite difference simulation, seismic wave propagation can be handled up to 3 Hz with a sampling of 2.26 grid points for the shortest wavelength in the horizontal directions and 4.53 grid points in the vertical direction, which are still effective for the higher-order scheme used [*Furumura and Chen*, 2004].

[80] The source-slip model for the event is approximated by a point double-couple source rather than a complex source rupture model; since our main concern is to understand the propagation path effects associated with random structure of the subduction zone and to demonstrate the waveguide effect of the subducted plate for higher frequencies, rather than concentrate on the detailed radiation from a complex source. The results of the source inversion study for this earthquake using far-field waveform data [*Yamanaka*, 2003] indicate that the deep, in-plate event can be almost represented by a point double-couple source and an impulsive source time function. We therefore used the seismic source of a pseudo-delta function which imparts seismic waves with a maximum frequency of 3 Hz. The simulation results are finally convolved with a proper source time function of *Nakamura and Miyatake* [2000] for the M_w 6.4 in-plate source to compare with observations.

[81] For such a large scale simulation we have employed the Earth Simulator supercomputer with a suitable parallel finite difference code for a large scale modeling of seismic wave propagation and a visualization of 3-D seismic wave field [*Furumura and Chen*, 2004]. By making full use of the vector hardware of the Earth Simulator, the 3-D finite difference simulation achieved a very good performance of over 40% of the peak processor performance (8 GFLOPS/CPU). The parallel simulation is based on the traditional domain partitioning procedure [*Furumura et al.*, 1998], where the 3-D model is partitioned vertically into a number of subregions assigned to many processors for concurrent computing and a message passing interface (MPI) is used to exchange data between neighbor processors. We confirmed that the parallel finite difference simulation achieves very good speed-up even using a large number of processors. The present simulation took a computer memory of about 1.3 TByte and CPU time of 1 hour using 1920 processors of the Earth simulator to calculate wave propagation for an interval of 250 s with time integration over 25,000 time steps.

[82] The 3-D simulations have been conducted using a set of different structural models, with the inclusion or exclusion of the subducting plate and mantle wedge and heterogeneity in the plate, to try to understand the contribution of each part of the model to the transmission of higher-frequency waves and the generation of anomalous intensity zones above the plate.

[83] As noted previously the pattern of regional intensity is mainly controlled by the absorption structure of the crust and the upper mantle structure including the subducting plate. However, site amplification effects due to low-wave speed superficial layer such as at deep sedimentary basins may also be important to explain some pockets of localized large intensities. Such effects, however, cannot included in our 3-D model due to grid size limitations (0.25 km in depth), and so we compensate by applying site amplification coefficients derived empirically from the relation of

surface geology and observations at (KiK-net) borehole stations [*Kubo et al.*, 2003] (Figure 17a). The site amplification coefficients applied to the simulations range from 1 (hard rock site) to 2.50 (soft sediment).

5.2. Simulation Results

[84] Simulation results are shown in Figures 18, 19, and 20 with snapshots of seismic wave propagation, intensity patterns, waveforms for different plate model and comparisons with observations. Snapshots of seismic wave propagation, extracted from the 3-D simulation for a model with no Pacific plate are shown in Figure 18a at 26, 56, and 118 s after source initiation. The corresponding results for a model with the Pacific plate including stochastic fluctuations in elastic constants are displayed in Figure 18b.

[85] In the first frame (26 s) of Figure 18a the *P* and *S* waves radiating from the source in the mantle at 360 km deep produce large ground motions above the hypocenter. The *P* and *S* waves propagating in central Japan attenuates gradually with propagation in the crust and upper mantle (56 and 118 s).

[86] When the source initiates inside the Pacific plate, the guiding of seismic waves in the high-wave speed and low-*Q* plate leads to significant *P* and *S* waves propagating to the north along the subducting plate at a higher speed than in the surrounding mantle [Figure 18b, 56 s, 118 s]. The high *Q* in the plate helps to sustain the multiple scattering for higher-frequency waves inside the plate giving rise to an extended high-frequency *P* and *S* wave coda in the last frame (118 s) that demonstrates clearly the scattering waveguide effect from 3-D plate structure. There are clear contrasts in the character of the wave propagation with station position relative to the volcanic front. Amplitudes are stronger on the Pacific Ocean side (forearc side) compared to the Japan Sea (back arc) side where the high-frequency signals attenuate significantly by traveling in the low-wave speed and low *Q* mantle wedge.

[87] Figure 19 compares the simulated intensity, in terms of the JMA scale, derived from 3-D finite difference simulation for different subduction zone models (Figures 19a–19c) with the observed intensity (Figure 19d) derived from the dense seismic arrays (K-NET and KiK-net).

[88] The first simulation uses a laterally heterogeneous crustal structure, excluding the subducting plate and the low-wave speed and low-*Q* wedge mantle. This produces a broad pattern of near constant seismic intensity above the hypocenter, with a maximum intensity of 2 above the hypocenter (Figure 19a). A pocket of larger intensity is also found in Tokyo, about 400 km from the hypocenter, due to the larger site amplification effects in the basin of Tokyo.

[89] With the introduction of the high-wave speed and high-*Q* subducting plate and the low-wave speed and low-*Q* materials in the wedge mantle, the area of larger intensity migrates significantly from the hypocenter by several hundred kilometers to the north (Figure 19b). The efficient propagation of high-frequency signals along the plate produces larger intensity of 3 in central Japan. The incorporation of the low-wave speed and low-*Q* wedge mantle dramatically attenuates the seismic waves above the hypocenter and at western seaboard (back arc side) of central Japan, which also enhances the anomalous extension of seismic intensities in eastern coastal side.

[90] The introduction of stochastic fluctuations in the plate and lower crust with elongated scatterers with a similar style to the 2-D simulations, produces scattering waveguide effects (Figure 19c). The resulting intensity anomalies reproduce the observations of the 12 November 2003 event (Figure 19a) reasonably well, with an extension of isoseismal contours to the north along eastern seaboard and significant loss of intensity on the back arc side. The simulated pattern does not extended the larger intensity zone to Tohoku and Hokkaido as seen in the observations. This discrepancy is likely to be due to the high-frequency bound ($f > 3$Hz) in the present 3-D simulation and the limitation of the discretization (0.5 km by 0.25 km) for representing the smaller scale heterogeneities in the plate (i.e., the correlation distance of 0.5 km in plate thickness).

[91] Synthetic waveforms at four broadband stations (TGA, TYM, KZK, and HRO) in the simulation area are compared with observed waveforms in Figure 20 for a models of flat plate structure with a high-*Q* and high-wave speed layer (as in Figure 19b) and the heterogeneous plate model with stochastic random fluctuations (as in Figure 19c). The simulated waveforms for the stochastic random fluctuations in plate structure explain the main characteristics of the observed waveforms at the forearc stations (HRO, TYM) fairly well, with large high-frequency signals and long duration of *P* and *S* wave coda. On the other hand, the simulation results using the simple plate model shows much simpler waveforms for forearc stations and very short *P* and *S* wave coda.

[92] The results of the simulations for this deep in-plate event indicate that 3-D simulations using current parallel computer can almost reach the level required to simulate high-frequency seismic waves not only for the major *P* and *S* phases but also for the shape of later phases. However, the separation of low-frequency precursor and high-frequency later signals is not clearly reproduced in the current simulation due to the lack of high-frequency signals over 3 Hz. As we have seen in the observations (Figures 7 and 5) the high-frequency scattered component is most prominent for frequencies higher than 2 Hz. The 3 Hz highest frequency we can reach with the current 3-D simulation is thus marginal for the high-frequency component and this contributes to the difference between observations and predictions in Figure 19. The 3-D calculations are quite sensitive to the details of the of the geometry of the geometry of the subduction zone and we may also need to improve the representations of Pacific plate structure.

[93] The stochastic heterogeneity in the 3-D case is a simple extension of that employed in 2-D, but if, as is likely, the pattern is imposed in the oceanic lithosphere by mid-ocean ridge processes, a larger correlation length would be appropriate parallel to the trend of the magnetic anomalies. Subduction of the Pacific plate is slightly oblique at the trench along the northern coast of the Japanese main island (Honshu). The combination of obliquity and anisotropic correlation properties could help to extend the region of larger intensity to the north in the example in Figure 19. Higher frequency calculations

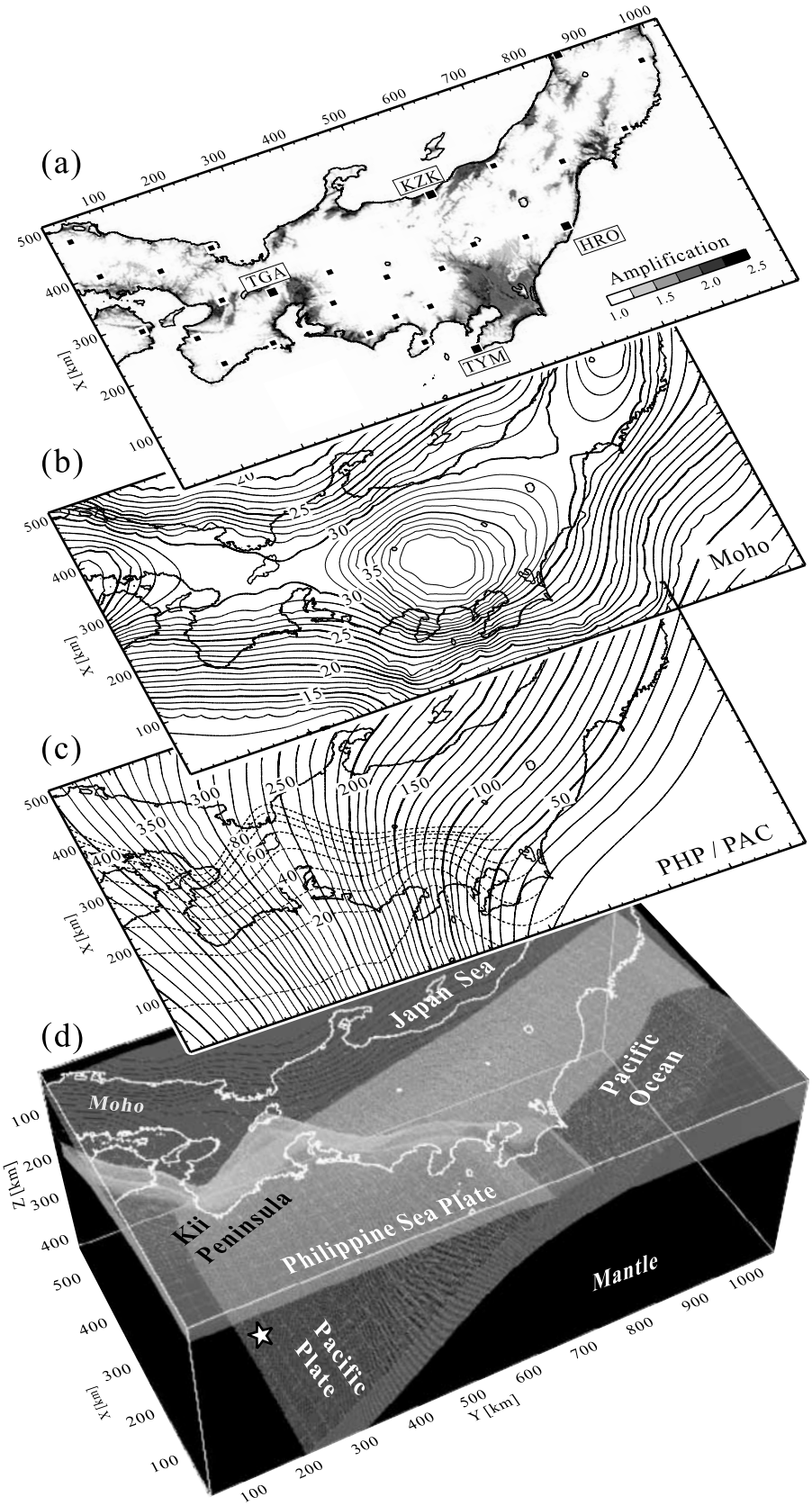

Figure 17. Structural model for northern Japan used in the 3-D simulation of seismic wave propagation, showing (a) Compensation coefficients for site amplification, (b) configuration of Moho, (c) the Pacific sea plate and the Philippine sea plate, and (d) 3-D view of the simulation model. Hypocenter is shown in star.

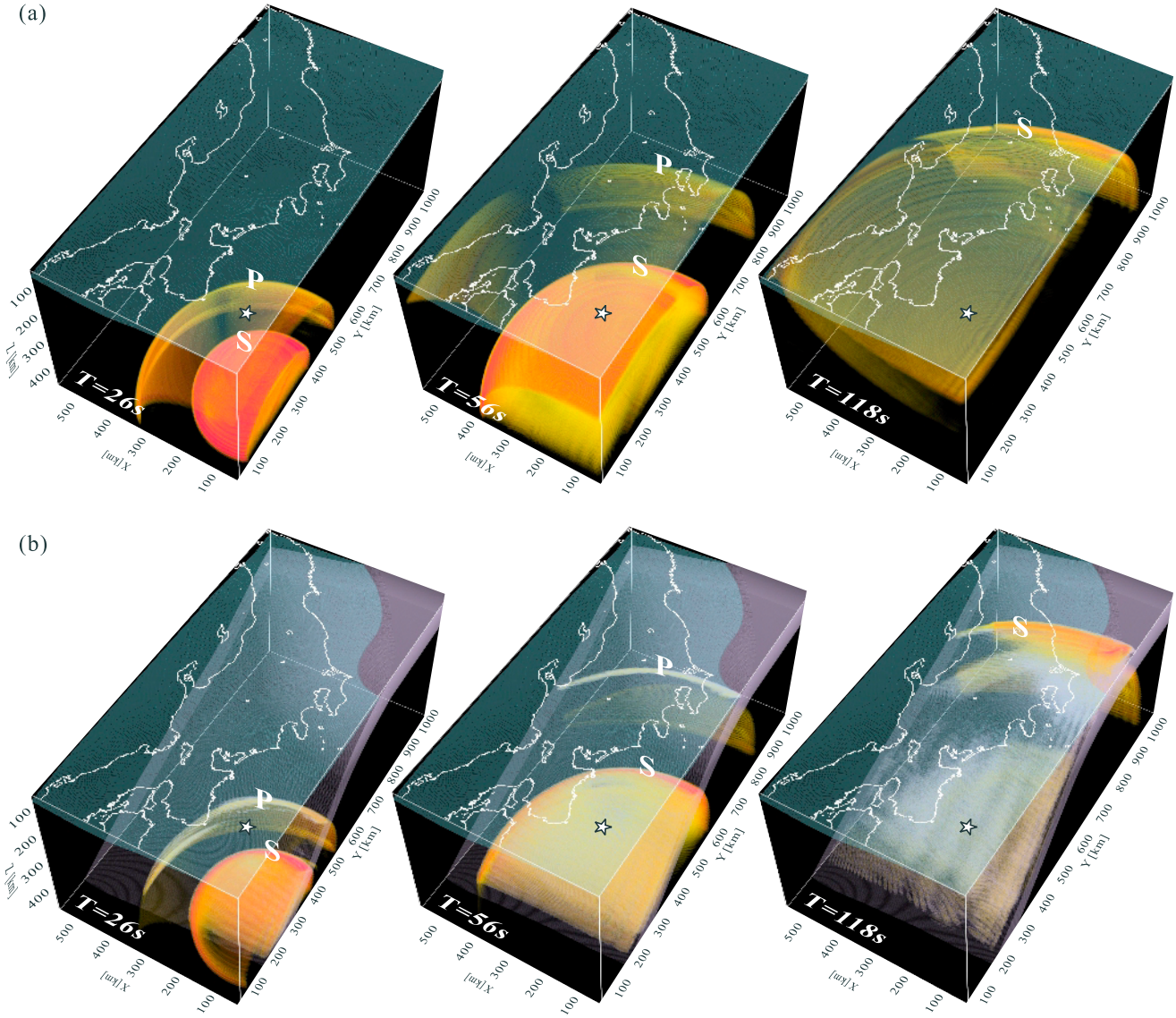

Figure 18. Snapshots of seismic wave propagation in 3-D heterogeneous structure of northern Japan derived from 3-D simulation, at 26, 56, and 118 s after source initiation, for (a) laterally heterogeneous structure excluding high-Q and high-wave speed plate and low-Q and low-wave speed wedge mantle and (b) full plate model including stochastic heterogeneity and the low-Q mantle wedge. Darker colors indicate larger energy in the wave fronts. P and S signals are marked.

would really be need to justify the inclusion of these extra effects.

6. Discussion and Conclusions

[94] The anomalously large intensity and very long duration of high-frequency seismic signals observed on the eastern seaboard of northern Japan from deep Pacific plate earthquakes is produced by the guiding of high-frequency seismic waves in the heterogeneous subducted plate, due to multiple internal scattering of seismic waves.

[95] Since the work of *Utsu* [1966] it has been recognized that the larger intensity on the eastern seaboard of Japan requires the presence of a large contrast in absorption structure between a low attenuation (high Q) subducting plate and a high-attenuation (low Q) mantle wedge. However, this simple model is not sufficient to explain the detailed characteristics of the three-component waveforms in the region of higher intensity, particularly the frequency-selective propagation.

[96] We have been able to show from numerical simulations of higher-frequency seismic waves to 18 Hz in 2-D models that the character of the observations can be matched when the plate heterogeneity is anisotropic with elongated structures along the downdip direction of the plate and much shorter scales in the plate thickness. Seismic waves with wavelength shorter than the short correlation distances in this class of stochastic laminated structure will be trapped in the waveguide due to multiple postcritical reflections that leads to a very long coda in all three components of motion. The high Q in the subducting plate also helps to sustain the amplitude of high-frequency signals

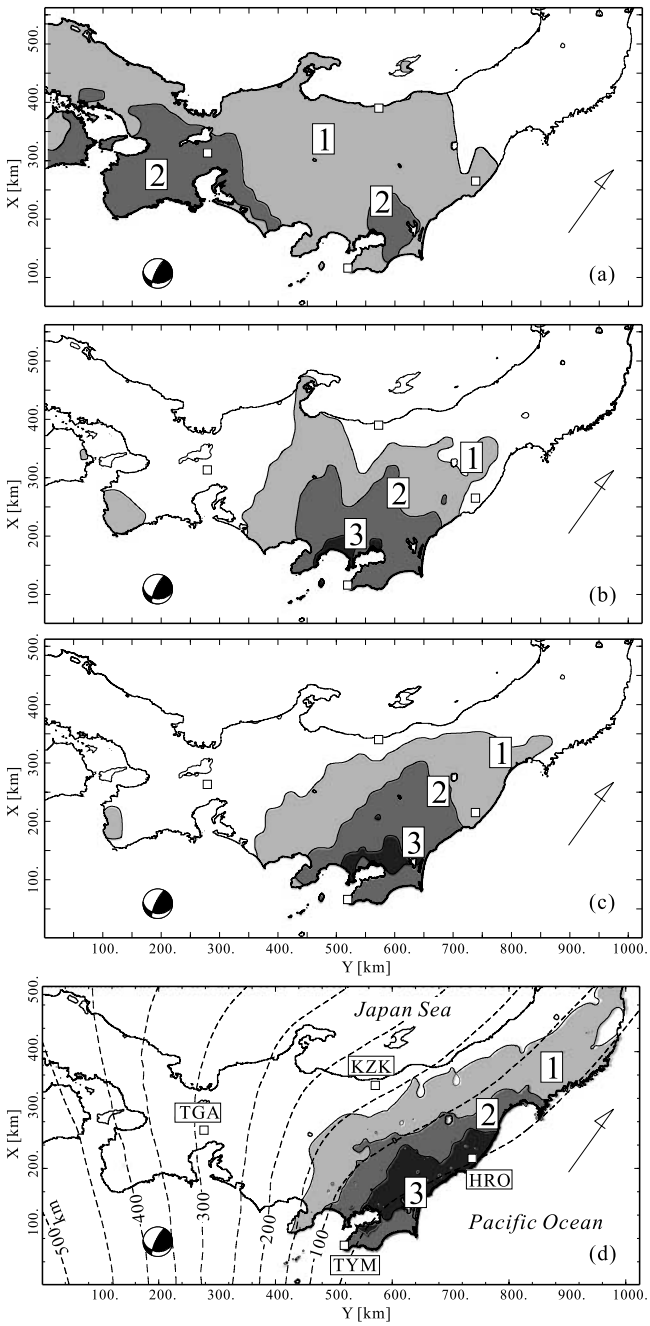

Figure 19. Simulated intensity distribution for the 12 November 2003 (M_w 6.4) event to the southeast of Kii Peninsula derived from the 3-D calculations using different plate models with (a) laterally heterogeneous crust, (b) inclusion of the high-Q Pacific plate and low-Q wedge mantle, (c) incorporation of randomly fluctuated plate, and (d) observed intensity pattern from KiK-net and K-NET data. The dashed lines represent the depth contours of the subducting Pacific plate. The locations of broadband stations (TGA, TYM, KZK, HRO) are shown.

for long distances. Low-frequency waves, with longer wavelength, can easy tunnel through the lamella features as like an inhomogeneous waves with the angle of incidence larger than the critical angle [*Fuchs and Schulz*, 1976].

[97] This new plate model with a scattering waveguide, is more complex than the simple traditional model with high Q and elevated wave speeds, but can simulate the observations mentioned above very well. The low-wave speed channel effect provided by the former oceanic crust can enhance the presence of high-frequency guided waves along the plate, but it is not the dominant contributor to ducting of the scattered high-frequency waves from deep events.

[98] The elongate heterogeneity structure appears to be an intrinsic property of the oceanic lithosphere carried with it into the subduction zone. Such heterogeneity would most likely be imposed as the oceanic plate grows away from the mid-ocean ridge, through sill injection and underplating processes as the lithosphere is formed. The required scale lengths are such that the horizontal gradients in lithospheric properties are small, and when sampled by reflection profiling would show little reflectivity. Simulations of seismic wave propagation through the oceanic lithosphere show that the same class of elongate heterogeneity structure is able to sustain *Pn*, *Sn* waves with complex codas to great distances as required by the observations of *Walker* [1977, 1981] across the Pacific Ocean basin.

[99] Comparisons between observed broadband waveforms and computer simulations of the scattering waveguide effect in the Pacific plate indicate that the characteristics of the observations are well matched by stochastic fluctuations in elastic parameters described by a von Karmann function with a long downdip correlation distance of about 10 km and a much small correlation distances of about 0.5 km across the thickness of the plate, the standard deviation from the background averaged model is about 2%. However, the actual situation is likely to be even more complex with variation in the nature of the heterogeneity through the thickness of the subduction zone, but this cannot be resolved from the available observations. Irrespective of the precise distribution, it is clear that structures elongated downdip are required to set up trapping of high-frequency energy in a region of generally elevated wave speeds.

[100] Events from the front of the Banda Sea arc recorded in northern Australia show a similar pattern of low-frequency onset followed by an extended high-frequency coda [*Kennett*, 1985, 1987]. This suggests that trapped energy within the subducted plate can be transmitted into the continental lithosphere that now abuts the trench and then travel long distances (1200 km) within a high Q but heterogeneous waveguide.

[101] Recent studies of the densely sampled observations along the long-range refraction experiment in the former Soviet Union using nuclear sources, have demonstrated the presence of large teleseismic *Pn* and *Sn* phases with extensive codas [e.g., *Tittgemeyer et al.*, 1990; *Morozova et al.*, 1999; *Nielsen and Thybo*, 2003; *Nielsen et al.*, 2003; *Ryberg et al.*, 2000]. The various models suggested to explain the observations all required horizontally extended structures. There are competing views on the balance and scale lengths of such heterogeneity between the lower crust and uppermost mantle, particularly because the continental mantle lithosphere appears to have little near vertical reflectivity.

[102] Separation of the high- and low-frequency components of the waveform is reported for other subduction zones, such as the Nazca plate at South America [*Snoke et*

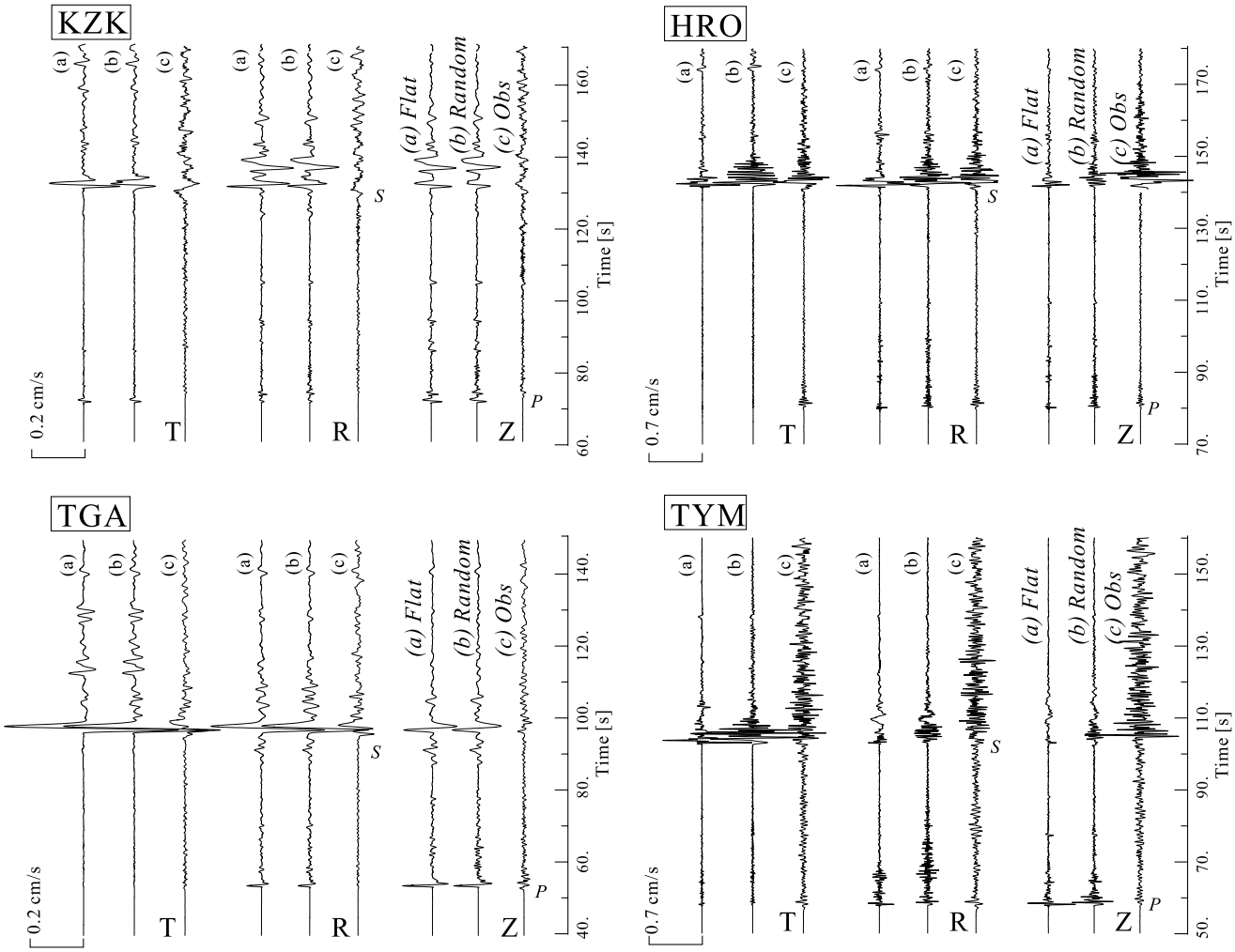

Figure 20. (a) Observed velocity records for vertical (Z), radial (R), and transverse (T) components of the 12 November 2003 earthquake for major broadband stations at forearc (HRO and TYM) and back arc side (KZK and TGA) of central Japan (see Figure 19d), are compared with waveforms from 3-D calculations for subduction models with (b) flat and (c) random plates.

al., 1974; *Martin et al.*, 2003], the Vanuatu region [*Chiu et al.*, 1985], and the Cocos plate off Nicaragua [*Abers et al.*, 2003], and ocean bottom seismographs at the Mariana Basin [*Ouchi*, 1981]. Anisotropic heterogeneity in the plate structure as we have described is therefore likely to be a common characteristic of most oceanic plates.

[103] In contrast to the early arrival of low-frequency waves for the deep events in the Pacific plate, earthquakes from the Tonga-Kermadec seismic zone recorded in New Zealand shows a very different pattern of observations with an early arrival with a high-frequency emergent signal and an impulsive low-frequency later arrival [*Gubbins and Snieder*, 1991; *Ansell and Gubbins*, 1986; *Smith et al.*, 1994; *van der Hilst and Snieder*, 1996]. This propagation along the plate indicates a different style of waveguide phenomena, but again heterogeneity within the plate provides a mechanism for extending the duration of the high-frequency component.

[104] The dense configuration of high-quality seismic stations in Japan will allow the capture of more waveforms from deep plate earthquakes, and should provide further insights into the heterogeneity structure of the subducting plate and the history of their development. For the shallowly dipping subduction of the Philippine sea plate the observations of anomalous intensity pattern in western Japan are much less clear [e.g., *Ikami and Ito*, 1974; *Utsu*, 1969; *Koketsu and Furumura*, 2002] and we may hope to understand the differences in the heterogeneity structure between two plates with a thick (80 km), old (120 Ma) Pacific plate and a thin (20 km), young (20 Ma) Philippine sea plate.

[105] Large-scale parallel 3-D simulation of seismic wave propagation using the Earth Simulator supercomputer has demonstrated the significance of the subduction zone structures beneath the Japanese Islands in controlling the pattern of intensity from deep events. Relatively high frequency wave propagation (3 Hz) has been achieved, so that the influence of heterogeneity in the subducted plate on anomalous patterns of seismic intensity can be recognized. The results of the 3-D simulation show clear waveguide effects for high-frequency signals traveling in the subducting plate due to internal multiple scattering. However, the simulations are not yet able to reproduce the typical feature of the observations from deep plate events with a separation of a

low-frequency precursor and later high-frequency signals with a long coda.

[106] As computational power continues to improve we hope to be able to carry the 3-D calculations to significantly higher frequencies with a finer grid model to provide a better representation of small-scale stochastic heterogeneities, and thereby narrow the gap between simulation and observations.

[107] **Acknowledgments.** This study was supported by a grant-in-aid from Japan Society of Promotion Science (JSPS) for a foreign research exchange fellowship between Japan and Australia. The computations were conducted as a joint research project "Seismic wave propagation and strong ground motions in 3-D heterogeneous structure" between the Earthquake Research Institute, University of Tokyo, and the Earth Simulator Center. We acknowledge the National Research Institute for Earth Science and Disaster Prevention (NIED) for the use of K-NET, KiK-net, and FREESIA waveform data. Constructive discussions with T. Sasatani, K. Suyehiro, Y. Fukao, T. Iidaka, J. Kawahara, A. Matsuzawa, and M. Hoshiba provided insights into the character of seismic signals in random media. Careful reviews and constructive comments from two anonymous reviewers and the Associate Editor were very helpful for revision of the manuscript.

References

Abers, G. A. (2000), Hydrated subducted crust at 100–250 km depth, *Earth Planet. Sci. Lett.*, *176*, 323–330.

Abers, G. A., T. Plank, and B. R. Hacker (2003), The wet Nicaraguan slab, *Geophys. Res. Lett.*, *30*(2), 1098, doi:10.1029/2002GL015649.

Aki, K., and B. Chouet (1975), Origin of coda waves: Source, attenuation and scattering effects, *J. Geophys. Res.*, *80*, 3322–3342.

Ansell, J. H., and D. Gubbins (1986), Anomalous high-frequency wave propagation from the Tonga-Kermadec seismic zone to New Zealand, *Geophys. J. R. Astron. Soc.*, *85*, 93–106.

Barazangi, M., B. Isacks, and J. Oliver (1972), Propagation of seismic waves through and beneath the lithosphere that descends under Tonga island arc, *J. Geophys. Res.*, *77*, 952–958.

Cerjan, C., D. Kosloff, R. Kosloff, and M. Reshef (1985), A nonreflecting boundary condition for discrete acoustic and elastic wave equations, *Geophysics*, *50*, 705–708.

Chiu, J.-M., B. L. Isacks, and R. K. Cardwell (1985), Propagation of high-frequency seismic waves inside the subducted lithosphere from intermediate-depth earthquakes recorded in the Vanuatu arc, *J. Geophys. Res.*, *90*, 12,741–12,754.

Ferris, A., G. A. Abers, D. H. Christensen, and E. Veenstra (2003), High resolution image of the subducted Pacific(?) plate beneath central Alaska, 50–150 km depth, *Earth Planet. Sci.*, 575–588.

Frankel, A. (1989), A review of numerical experiments on seismic wave scattering, *Pure Appl. Geophys.*, *131*, 639–685.

Frankel, A., and R. W. Clayton (1984), A finite-difference simulation of wave propagation in two-dimensional random media, *Bull. Seismol. Soc. Am.*, *74*, 2167–2186.

Fuchs, K. (1977), Seismic anisotropy of the subcrustal lithosphere as evidence for dynamical processes in the upper mantle, *Geophys. J. R. Astron. Soc.*, *49*, 167–179.

Fuchs, K., and K. Schulz (1976), Tunneling of low-frequency waves through the subcrustal lithosphere, *J. Geophys.*, *42*, 175–190.

Fukao, Y., S. Hori, and M. Ukawa (1983), A seismological constraining on the depth of basalt-ecologite transition in a subducting oceanic crust, *Nature*, *303*, 413–415.

Furumura, T., and L. Chen (2004), Large scale parallel simulation and visualization of 3-D seismic wavefield using the Earth simulator, *Comput. Model. Eng. Sci.*, *6*, 153–168.

Furumura, T., B. L. N. Kennett, and H. Takenaka (1998), Parallel 3-D pseudospectral simulation of seismic wave propagation, *Geophysics*, *63*, 279–288.

Furumura, T., K. Koketsu, and K.-L. Wen (2001), Parallel PSM/FDM hybrid simulation of ground motions from the 1999 Chi-Chi, Taiwan, earthquake, *Pure Appl. Geophys.*, *159*, 2133–2146.

Gubbins, D., and R. Snieder (1991), Dispersion of *P* waves in subducted lithosphere: Evidence for an ecologite layer, *J. Geophys. Res.*, *96*, 6321–6333.

Hasegawa, K. (1918), An earthquake under the Sea of Japan, *J. Meteorol. Soc. Jpn.*, *37*, 203–207.

Hori, S., H. Inoue, Y. Fukao, and M. Ukawa (1985), Seismic detection of the untransformed 'basaltic' oceanic crust subducting into the mantle, *Geophys. J. R. Astron. Soc.*, *83*, 169–197.

Iidaka, T., and M. Mizoue (1991), *P*-wave velocity structure inside the subducting Pacific plate beneath the Japan region, *Phys. Earth Planet, Inter.*, *66*, 203–231.

Ikami, A., and K. Ito (1974), Seismic waves traveling from southwest Japan to Inuyama Seismological Observatory, *J. Seismol. Soc. Jpn.*, *2*(27), 225–238.

Ikelle, L., S. K. Yung, and F. Daube (1993), 2D random media with ellipsoidal autocorrelation functions, *Geophysics*, *58*, 1359–1372.

Isacks, B. L., and M. Barazangi (1973), High frequency shear waves guided by a continuous lithosphere descending beneath western South America, *Geophys. J. R. Astron. Soc.*, *33*, 129–139.

Ishikawa, T. (1926a), On the abnormal distribution of felt areas of an earthquake, *J. Meteorol. Soc. Jpn., Ser. 2*, *4*, 137–146.

Ishikawa, T. (1926b), On seismograms of earthquakes exhibiting abnormal distribution of seismic intensities, *Q. J. Seismol.*, *2*, 7–15.

Ishikawa, T. (1930), Über die Anormale Ershüterngsgebiete der Erdberben, *Geophys. Mag.*, *3*, 95–100.

Ishikawa, T. (1933), The abnormal distribution of seismic intensities, 2 (in Japanese), *Q. J. Seismol.*, *7*, 37–70.

Katsumata, K., N. Wada, and M. Kasahara (2003), Newly imaged shape of the deep seismic zone within the subducting Pacific plate beneath the Hokkaido corner, Japan-Kurile arc-arc junction, *J. Geophys. Res.*, *108*(B12), 2565, doi:10.1029/2002JB002175.

Kennett, B. L. N. (1985), On regional *S*, *Bull. Seismol. Soc. Am.*, *75*, 1077–1088.

Kennett, B. L. N. (1987), Observational and theoretical constraints on crustal and upper mantle heterogeneity, *Phys. Earth Planet. Inter.*, *47*, 319–332.

Kennett, B. L. N., E. R. Engdahl, and R. Buland (1995), Constraints on the velocity structure in the Earth from travel times, *Geophys. J. Int.*, *122*, 108–124.

Koketsu, K., and T. Furumura (2002), The distribution of strong ground motion from the 2001 Geiyo earthquake and the deep underground structure (in Japanese), *J. Seismol. Soc. Jpn.*, (55), 97–105.

Kubo, T., Y. Hisada, A. Shibayama, M. Ooi, M. Ishida, H. Fujiwara, and K. Nakayama (2003), Development of digital maps of site amplification factors in Japan, and their application to early strong motion estimations (in Japanese), *J. Seismol. Soc. Jpn.*, (56), 21–37.

Marcinkovich, C., and K. Olsen (2003), On the implementation of perfectly matched layers in a three-dimensional fourth-order velocity-stress finite difference scheme, *J. Geophys. Res.*, *108*(B5), 2276, doi:10.1029/2002JB002235.

Martin, S., A. Rietbrock, C. Haberland, and G. Asch (2003), Guided waves propagating in subducted oceanic crust, *J. Geophys. Res.*, *108*(B11), 2536, doi:10.1029/2003JB002450.

Matsuzawa, T., N. Umino, A. Hasegegawa, and A. Takagi (1987), Estimation of thickness of a low-velocity layer at the surface of the descending oceanic plate beneath the northeastern Japan arc by using synthesized *PS*-wave, *Tohoku Geophys. J.*, *31*, 19–28.

Morozova, E. A., I. B. Morozov, S. B. Smithson, and L. N. Solodilov (1999), Heterogeneity of the uppermost mantle beneath Russian Eurasia from the ultra-long range profile QUARTZ, *J. Geophys. Res.*, *104*, 20,329–20,348.

Nakamura, H., and T. Miyatake (2000), An approximate expression of slip velocity time function for simulation of near-field strong ground motion, *J. Seismol. Soc. Jpn.*, *53*, 1–9.

Nielsen, L., and H. Thybo (2003), The origin of teleseismic *Pn* waves: Multiple crustal scattering of upper mantle whispering gallery phases, *J. Geophys. Res.*, *108*(B10), 2460, doi:10.1029/2003JB002487.

Nielsen, L., H. Thybo, A. Levander, and N. Solodilov (2003), Origin of upper-mantle seismic scattering - evidence from Russian peaceful nuclear explosion data, *Geophys. J. Int.*, *154*, 196–204.

Oda, H., T. Tanaka, and K. Seya (1990), Subducting oceanic crust on the Philippine sea plate in southwestern Japan, *Tectonophysics*, *172*, 175–189.

Ouchi, T. (1981), Spectral structure of high frequency *P* and *S* phases observed by OBS's in the Mariana basin, *J. Phys. Earth*, *29*, 305–326.

Robertsson, J. O. A., J. O. Blanch, and W. W. Symes (1994), Viscoelastic finite-difference modeling, *Geophysics*, *59*, 1444–1456.

Ryberg, T., M. Tittgemeyer, and F. Wenzel (2000), Finite-difference modelling of *P*-wave scattering in the upper mantle, *Geophys. J. Int.*, *141*, 787–800.

Ryoki, R. (1999), Three-dimensional depth structure of the crust and uppermost mantle beneath southwestern Japan and its regional gravity anomalies, *J. Seismol. Soc. Jpn.*, *52*, 51–63.

Smith, G., D. Gubbins, and W. Mao (1994), Fast *P* wave propagation in subducted Pacific lithosphere: Reflection from the plate, *J. Geophys. Res.*, *99*, 23,787–23,800.

Snoke, J. A., I. S. Sacks, and H. Okada (1974), A model not requiring continuous lithosphere for anomalous high-frequency arrivals from

deep-focus South American earthquakes, *Phys. Earth Planet. Inter.*, *9*, 199–206.

Takanami, T., I. S. Sacks, and A. Hasegawa (2000), Attenuation structure beneath the volcanic front in northeastern Japan from broad-band seismograms, *Phys. Earth Planet. Inter.*, *121*, 339–357.

Tittgemeyer, M., F. Wenzel, T. Ryberg, and K. Fuchs (1990), Scales of heterogeneities in the continental crust and upper mantle, *Pure Appl. Geophys.*, *156*, 29–52.

Tsumura, N., S. Matsumoto, S. Horiuchi, and A. Hasegawa (2000), Three-dimensional attenuation structure beneath the northeastern Japan arc estimated from spectra of small earthquakes, *Tectonophysics*, *319*, 241–260.

Utsu, T. (1966), Regional difference in absorption of seismic waves in the upper mantle as inferred from abnormal distribution of seismic intensities, *J. Fac. Sci. Hokkaido Univ., Ser. VII*, *2*, 359–374.

Utsu, T. (1967), Anomalies in seismic wave velocity and attenuation associated with a deep earthquake zone (I), *J. Fac. Sci. Hokkaido Univ., Ser. VII*, *3*, 1–25.

Utsu, T. (1969), Anomalous seismic intensity distributions in western Japan, *Geophys. Bull. Hokkaido Univ.*, *21*, 45–52.

Utsu, T., and H. Okada (1968), Anomalies in seismic wave velocity and attenuation associated with a deep earthquake zone (II), *J. Fac. Sci. Hokkaido Univ., Ser. VII*, *3*, 65–84.

van der Hilst, R., and R. Snieder (1996), High-frequency precursors to *P* wave arrivals in New Zealand: Implications for slab structure, *J. Geophys. Res.*, *101*, 8473–8488.

Wadati, K. (1928), Shallow and deep earthquakes, *Geophys. Mag.*, *1*, 162–202.

Walker, D. (1977), High frequency *Pn* and *Sn* phases recorded in the western Pacific, *J. Geophys. Res.*, *82*, 3350–3360.

Walker, D. (1981), High frequency *Pn* and *Sn* velocities: Some comparisons for the western, central and south Pacific, *Geophys. Res. Lett.*, *9*, 207–209.

Yamanaka, Y. (2003), EIC seismological note no.143: Offshore Kii Peninsula earthquake of 12 Nov. 2003 (M_J6.5). (available at http://www.eri.u-tokyo.ac.jp/sanchu/Seismo_Note/EIC_News/EIC142.html)

Yamazaki, F., and T. Ooida (1985), Configuration of subducted Philippine sea plate beneath the Chubu distinct, central Japan, *J. Seismmol. Soc. Jpn.*, *38*, 193–201.

Yuan, X., et al. (2000), Subduction and collision processes in the central Andes constrained by converted seismic phases, *Nature*, *408*, 958–961.

Zhao, D. A., and A. Hasegawa (1993), *P* wave tomographic imaging of the crust and upper mantle beneath the Japan Islands, *J. Geophys. Res.*, *98*, 4333–4353.

T. Furumura, Earthquake Research Institute, University of Tokyo, 1-1-1 Yayoi, Bunkyo-ku, 113-0032, Japan. (furumura@eri.u-tokyo.ac.jp)

B. L. N. Kennett, Research School of Earth Sciences, Australian National University, Canberra ACT 0200, Australia. (brian@rses.anu.edu.au)